High-quality 3D shape measurement with binarized dual phase-shifting method

by

Saptarshi Basu

A thesis submitted to the graduate faculty in partial

fulfillment of the requirements for the degree of

MASTER OF SCIENCE

Major: Mechanical Engineering

Program of Study Committee:
Beiwen Li, Major Professor
Abhijit Chandra
James H Oliver

The student author, whose presentation of the scholarship herein was approved by the program of study committee, is solely responsible for the content of this thesis. The Graduate College will ensure this thesis is globally accessible and will not permit alterations after a degree is conferred.

Iowa State University

Ames, Iowa

2018

Copyright © Saptarshi Basu, 2018. All rights reserved.

DEDICATION

I would like to dedicate this thesis to Mom, Dad, my sister and brother-in-law for being there for me all these years. Love you all.

TABLE OF CONTENTS

Page

LIST OF FIGURES. v

ACKNOWLEDGEMENTS vii

ABSTRACT. ix

CHAPTER 1. INTRODUCTION. 1

1.1 Motivations 1

1.2 3-D Shape Measurement Techniques 3

1.2.1 Contact Techniques 4

1.2.2 Non-Contact Techniques 4

1.3 Objective. 16

1.4 Organization. 16

CHAPTER 2. BASIS OF 3-D SHAPE MEASUREMENT 18

2.1 Digital Fringe Projection (DFP) 18

2.2 Calibration. 19

2.2.1 Pinhole Model of the Structured Light System 21

2.2.2 Calibration Procedure. 23

2.3 3-D Reconstruction 26

2.3.1 Summary. 27

CHAPTER 3. BINARIZED DUAL PHASE-SHIFTING METHOD FOR HIGH QUALITY 3D SHAPE MEASUREMENT 28

3.1 Introduction 28

3.2Principle 30

3.2.1 Single Phase-shifting algorithm (SPS) 30

3.2.2 Dual phase-shifting algorithm (DPS) 30

3.2.3 Binarized dual phase-shifting algorithm (BDPS) 32
3.2.4 Hilbert binarized dual phase-shifting algorithm (HBDPS) 33
3.3 Experiments 34
3.4 Summary 38
CHAPTER 4. SUMMARY AND FUTURE SCOPE OF WORK. 40
4.1 Research Achievements 40
4.2 Future scope of work 41
BIBLIOGRAPHY. 45

LIST OF FIGURES

Page

Figure 1.1 Illustration of principle of Stereo Vision system 8

Figure 1.2 Concept of structured light technique. (a) Schematic diagram explaining the principle of structured light technique; (b) correspondence determination by finding the intersection point between phase line and epipolar line. 9

Figure 1.3 An example of pseudo random pattern. 10

Figure 1.4 An example set of patterns and associated codifications of the Binary coding method. 11

Figure 1.5 Concept of N-ary codification. (a) A example N-ary pattern; (b) a cross-section of (a) showing multiple gray levels. 12

Figure 1.6 Concept of sinusoidal codification. (a) A example sinusoidal pattern; (b) a cross-section of (a) showing the sinusoidal profile. 13

Figure 1.7 Working principle of Digital Light Processing method 15

Figure 1.8 Binary Projection at different defocusing levels with the first image being in-focus. The sinusoidal structures appear in the mid-level of defocusing. 16

Figure 2.1 An example procedure for the DFP technique. (a) - (c) Three-step phase shifted patterns; (d) wrapped phase; (e) unwrapped phase; (f) 3D reconstructed geometry. 20

Figure 2.2 Illustration of Pinhole camera model. 21

Figure 2.2 Illustration of Pinhole camera model. 21

Figure 2.3 An example of calibration board. 24

Figure 3.1 Phase errors induced by (2k + 1)th (k=1,2,3...) order harmonics. 31

Figure 3.2 Steps to generate a BDPS pattern. (a) An overlay of the cross-sections of the original and the π/6 shifted square binary pattern; (b) the average of the pattern cross-sections in (a) exhibiting three gray levels; (c) - (d) the original square binary pattern and the BDPS pattern, the BDPS pattern is generated by binarizing the middle graylevel shown in (b). 33

Figure 3.3 A simulation conducted to compare the performance of SPS, BDPS and HBDPS methods under different sizes of Gaussian smoothing filters (to emulate different projector defocusing levels). (a) The comparison of a cross section of the phase error maps when a small (3×3) Gaussian filter is applied; (b) a more thorough evaluation by comparing the rms errors at different sizes of Gaussian smoothing filters. 35

Figure 3.4 Phase error evaluation through measurement of a white planar surface. (a) - (c) Fringe images corresponding different projector defocusing degrees (in-focus, slightly defocused, significantly defocused); (e) - (h) corresponding phase errors plots. The RMS errors of (e) are 0.172 rad (SPS), 0.092 rad (BDPS) and 0.046 rad (HBDPS), respectively; the RMS errors of (f), the RMS errors are 0.088 rad (SPS), 0.031 rad (BDPS) and 0.019 rad (HBDPS), respectively; the RMS errors of (g), the RMS errors are 0.030 rad (SPS), 0.026 rad (BDPS) and 0.018 rad (HBDPS), respectively. 36

Figure 3.5 3D shape measurement of a sculpture head for visual comparison. (a) - (d) Figures showing the fringe image, the SPS result, the BDPS result and the HBDPS result when the projector is in-focus; (e) - (h) corresponding results when the projector is slightly defocused; (i) (l) corresponding results when the projector is significantly defocused. 39

ACKNOWLEDGEMENTS

First and foremost, I would like to express my heartiest gratitude to my advisor, Dr. Beiwen Li for allowing me to join his innovative group. Without whose support and motivation, it wouldn't have been possible for me to understand the various aspects of conducting research and the writing of this thesis. He has been very accommodating and always encouraged me to come to him whenever I needed his help. I am really very fortunate to be able to work alongside such a professor and for his guidance, patience and support throughout this research.

Moreover I would like to thank my committee members for their tremendous help: Dr. Abhijit Chandra, Dr. James H Oliver. Dr. Chandra has been always there for me throughout my ordeal. I am really grateful to him for his advice and support all these years as a teacher and the director of graduate education (DOGE) of the department. I thank Dr. Oliver for giving me a lot of sense and inspiration. He always welcomed me whenever I needed his advice and help. I wanted to thank all of you for your support and willingness to help in my time of need.

I would also like to convey my thanks to all other professors and my colleagues Vignesh Suresh and Jace Holton for willing to accommodate me and help me understand the concepts whenever I needed.

I would like to thank my parents my sister and my brother in law without whose efforts, encouragement & support, I wouldnt be standing where I find myself presently. Without their blessings, this academic endeavor couldnt have been accomplished. I would also like to thank all my relative, especially my Uncle Mr. Kalyan Biswas and my little nephew Vivaan, who have always been there for me.

Last but not the least I would like to thank Abhishek Sarkar and all my friends and seniors who has been my extended family here in Ames as well as in India. Thank you for all your support. I am very lucky to be able make such good friends like you.

ABSTRACT

3-D technology is a commonplace in today's world. They are used in many different aspects of life. Researchers have been keen on 3-D shape measurement and 3-D reconstruction techniques in past decades as a result of inspirations from different applications ranging from manufacturing, medicine to entertainment. The techniques can be broadly divided into contact and non-contact techniques. The contact techniques like coordinate measuring machine
(CMM) dates way back to 1950s. It has been used extensively in the industries since then. It becomes predominant in industrial inspections owing to its high accuracy in the order of μm. As we know that quality control is an important part of modern industries hence the technology is enjoying great popularity. However, the main disadvantage of this method is its slow speeds due to its requirement of point-by-point touch. Also, since this is a contact process, it might deform a soft object while performing measurements.

Such limitations led the researchers to explore non-contact measurement technologies (optical metrology techniques). There are a variety of optical techniques developed till now. Some of the well-known technologies include laser scanners, stereo vision, and structured light systems. The main limitation of laser scanners is its limited speed due to its point-bypoint or line-by-line scanning process. The stereo vision uses two cameras which take pictures of the object at two different angles. Then epipolar geometry is used to determine the 3-D coordinates of points in real-world. Such technology imitates human vision, but it had a few limitations too like the difficulty of correspondence detection for uniform or periodic textures. Hence structured light systems were introduced which addresses the aforementioned limitations. There are various techniques developed including 2-D pseudo-random codification, binary codification, N-ary codification and digital fringe projection

(DFP). The limitation of 2-D pseudo-random codification technique is its inability to achieve high spatial resolution since any uniquely generated and projected feature requires a span of several projector pixels. The binary codification techniques reduces the requirement of 2-D features to 1-D ones. However, since there are only two intensities, it is difficult to differentiate between the individual pixels within each black or white stripe. The other disadvantage is that n patterns are required to encode 2^n pixels, meaning that the measurement speeds will be severely affected if a scene is to be coded with high-resolution. Differently, DFP uses continuous sinusoidal patterns. The usage of continuous patterns addresses the main disadvantage of binary codification (i.e. the inability of this technique to differentiate between pixels was resolved by using sinusoid patterns). Thus, the spatial resolution is increased up to camera-pixel-level. On the other hand, since the DFP technique used 8-bit sinusoid patterns, the speed of measurement is limited to the maximum refreshing rate of 8-bit images for many video projectors (e.g. 120 Hz). This made it inapplicable for measurements of highly dynamic scenes. In order to overcome this speed limitation, the binary defocussing technique was proposed which uses 1-bit patterns to produce sinusoidal profile by projector defocusing. Although this technique has significantly boosted the measurement speed up to kHz-level, if the patterns are not properly defocused (nearly focused or overly defocused), increased phase noise or harmonic errors will deteriorate the reconstructed surface quality.

In this thesis research, two techniques are proposed to overcome the limitations of both DFP and binary defocusing technique: binarized dual phase shifting (BDPS) technique and Hilbert binarized dual phase shifting technique (HBDPS). Both techniques were able achieve high quality 3-D shape measurements even when the projector is not sufficiently defocused. The harmonic error was reduced by 47% by the BDPS method, and 74% by the HBDPS method. Moreover, both methods use binary patterns which preserve the speed advantage

of the binary technology, hence it is potentially applicable to simultaneous high-speed and high-accuracy 3D shape measurements.

CHAPTER 1. INTRODUCTION

1.1 Motivations

The three-dimensional (3-D) optical metrology has been studied extensively with potential applications in the field of manufacturing, entertainment and biomedical sciences. There has been more attentions regarding high density 3-D scanning performed at realtime or faster. In the past, it has been difficult to obtain the required hardware to realize such technology let alone to deploy the actual system. Nowadays with the advancement of innovative technical approaches, along with the advancements in hardware and software development, it has become possible to make these technologies commercially available.

To realize dense 3-D shape measurement at real-time or faster, it is worth investigating optical 3-D scanning techniques given their non-contact nature. Over the years, there has been a tendency toward getting higher data acquisition rate and higher measurement accuracies. A few associated current and potential applications are mentioned below:

Manufacturing and industrial applications. Metrology plays a big part in the industries. Accurate measurements are imperative nowadays. In general, micrometer level accuracy is needed in some industries such as aerospace, automotive industries, etc. Nowadays, with high competitiveness on market, the companies are striving to achieve higher production ability without compromising the quality of the products. There are methods like coordinate measuring machines (CMM) (to be discussed Section 1.2.1) can achieve a very high level of accuracy (Pfeifer and Effenkammer, 2000) which satisfies the industrial standard. However, this technique is typically slow given the fact that it is a contact technique, which may be inappropriate if a quick in-line inspection is required to reject some obviously bad parts. Hence the non-contact methods were developed to accommodate the needs. These

technologies can be used in various applications, which include surface roughness measurement, high-speed dimensional measurements, displacement measurements (Pettigrew, 1988), etc. The high speed optical measurement techniques can be useful in oil transportation and refining industry as well. Nowadays, with the level of advancement, the engineers are able to clearly trace and document changes over time in oil transportation vessels and the influence of additives and other techniques to prevent corrosion in the system using high-resolution 3D analysis (McGovern et al., 2002).

Bio-medical applications. 3-D imaging techniques are widely used in medical field for diagnostic purposes (Sansoni et al., 2009; Bitte et al., 2001). Some widely used techniques include CT scans and magnetic resonance imaging (MRI) which are able to conduct an accurate scanning of internal structures of human body. There are also medical applications where the surface topology information is tested to assist disease diagnosis. Associated technologies include facial anthropometry (Bush and Antonyshyn, 1996), 3D endoscopy imaging (Armbruster and Scheffler, 1998), etc. The facial anthropometry (Ferrario et al., 1998) is a technique which uses 3-D imaging to capture facial expressions. This could be used for cosmetic surgery or for detection of diseases like facial paralysis. Scientists have been trying to use structured light system for more than a decade to reconstruct the 3-D image of the face (Bhatia et al., 1994). These 3-D data from various frames of facial expressions can be used for diagnostic purposes (Mehta et al., 2008). A researcher has proposed anthropometric and anthroposcopic findings for primary lip and palate repair (Farkas et al., 1993). Olesen et al. (2012) (Olesen et al., 2012) were able to incorporate structured light system into a PET scanner for 3-D head motion tracking. 3D endoscopy imaging is another application where structured light can be incorporated. Endoscopy is the technique that is extensively used for diagnosis as well as surgical purposes. Scientist are trying to realize 3-D imaging capabilities (Armbruster and Scheffler, 1998) using the structured light system. This will allow the

doctors to be able to visually see the 3-D image of the infected area for better diagnosis. Both aforementioned applications require high-accuracy as well as high-speed. High-accuracy can improve the effectiveness of disease diagnosis given that the detected surface features of the moving subject (e.g. face, organs) can be better matched to some known patterns of diseases. Moreover, high-speed is also quite necessary. For instance, in the case of facial anthropometry, the dynamic facial expression is captured. So the technique should be able to capture subtle changes in real-time to improve effectiveness. Similarly, in the case of 3-D endoscopy, high-speed is crucial during a surgical process for real-time surveillance inside the body.

Entertainment industry and virtual reality. Nowadays, 3-D imaging techniques are pretty widespread in entertainment industries. There are not only 3-D movies, but also games being designed which are three-dimensional. The advancement in 3-D imaging techniques helped reduce the cost of production of such movies and games, enhance the user experience and increase the popularities. Moreoever, there are other applications of 3-D imaging like virtual classrooms, where students can access various courses (Menna et al., 2011; Gonzalez-Jorge et al., 2013, 2015; Pagliari et al., 2014).

Although optics is one of the earliest branches of physics, the use of optics in some of the applications (e.g. quality control and metrology) has a comparatively shorter history of several decades. In past decades, there has been an upsurge in research and development in a number of 3-D shape measurement techniques. The next section will provide a brief overview of existing 3-D shape measurement techniques.

1.2 3-D Shape Measurement Techniques

The 3-D shape measurement techniques can be broadly divided into **contact techniques** and **non-contact techniques**. The detailed descriptions of which are discussed below:

1.2.1 Contact Techniques

A coordinate measuring machine or CMM (McMurtry, 1982; Pettersson, 2009) is one of the most widely used contact techniques in the field of metrology. Here the object is subjected to physical touch by resting the object on a precision flat surface plate, and the 3-D coordinate of a certain point is determined by the physical location of the touch under the machine's coordinate system. The CMMs are used in manufacturing application for precision scanning. The CMMs are highly accurate given that they can achieve a measurement precision of 0.1 μm (Vermeulen et al., 1998). However, there are also various disadvantages of CMMs:

- The scanning procedure might deform the object surface being scanned as CMMs require physical contact with the object to be scanned.
- The scanning process is relatively slow due to its nature of point-by-point physical contact, which could take hours to scan a part with large surface area.

Given the aforementioned limitations of a CMM, it is not quite suitable if a quick decision needs to be made on some parts with obvious defects. Therefore, it is worth investigating non-contact optical techniques for 3-D shape measurements.

1.2.2 Non-Contact Techniques

Some major non-contact 3-D shape measurement techniques are reviewed as follows:

1.2.2.1 Laser Scanning

Based on different principles of scanning and 3D reconstruction, the laser scanning techniques can be divided into two broad categories:

a. **Time-of-flight (TOF) laser scanner**.

In this method, the laser pulse is emitted onto the object. Then a laser range finder is used to detect the reflected light from the object. The distance is estimated by the laser range finder based on the round-trip time taken by the emitted pulse to return after reflection from the object. Hence, if we consider that speed of light is c which is known and time taken by the laser for the round trip is t, then the depth information d is computed by

$$d = c \times t/2 \tag{1.1}$$

The laser scanners mostly modulate the light source at constant frequency and then measure the depth by determining the phase difference before and after the reflection of light. These scanners scan the entire field of view one point at a time by changing the direction of view of the range finder. The view direction of the range finder can be changed by rotating the range finder itself or by introduction of a system of rotating mirrors. A TOF scanner can measure a distance of 10,000 to 100,000 points per second. The main advantage of using these scanners is that they are very compact as the laser source and the receiver share the same viewing angle. However, there are shortcomings of this technology as well. The major limitation lies in its limited spatial and depth resolution. For instance, if a sub-millimeter depth resolution is to be achieved, a sensor resolution of less than 3.3 picoseconds needs to be reached.

b. **Triangulation-based 3D laser scanner.**

In this case, the system consists of a lens which is used to focus the laser beam on the object, an emitter and a detector (a camera). Here the emitter shines the laser beam on the object, which is then received by a camera which looks like either a dot or a line. The laser dots or lines are to be swept across the entire surface to get the surface

profile. This method is called triangulation given that the emitter, receiver and the laser dot/line form a triangle. The depth information can be calculated by examining the triangulation relationship. A major limitation of this method is that its measurement speed is constrained by the speed of dot or line scanning, and thus is not quite suitable for measuring a moving object.

1.2.2.2 Depth from Defocus (DFD)

It is a proven fact that the image captured by an optical system remains in focus till a certain distance from the optical axis after which the image gets out of focus (Subbarao, 1994). In real life cases, the images contain varied amount of blurring throughout the image. The surface profile of the object being captured can be determined by quantifying the extent of defocusing and then by relating it to depth information. In order to determine the depth from defocus, various images are captured at varied focus and aperture settings (Favaro and Soatto, 2005; Watanabe and Nayar, 1998; Favaro et al., 2008; Rajan and Chaudhuri, 2003; Rajagopalan and Chaudhuri, 1999). Hence, the points will have varied amount of blurring. So, if the blurring can be quantified, then the depth information can be recovered (Subbarao, 1994). Some scientists have used other sophisticated techniques (Levin et al., 2007; Namboodiri and Chaudhuri, 2008; Chen and Chen, 2011; Lin et al., 2013) to successfully create the 3-D image. The advantage of this method is its simple system setup as a single camera will be sufficient for image acquisition and 3-D reconstruction. However, there are also disadvantages associated with this method:

- More than one images with varied defocusing level is required for unique reconstruction of the scene (Favaro and Soatto, 2005).

- The sensitivity is usually not very high, as this technique requires strong texture information for analysis of the blurring effect (Schechner and Kiryati, 2000).

1.2.2.3 Stereo Vision

Stereo vision or stereopsis is a passive triangulation technique which requires ambient illumination (Dhond and Aggarwal, 1989). Stereo vision achieves the reconstruction of 3D structure or perception of depth based on visual information with normally developed binocular vision. Here, there are two cameras which captures 2-D images of the object from two different angles. The geometrical relationship between the 3-D points and the 2-D images is called **epipolar geometry** (Li, 2014; Scharstein and Szeliski, 2002). Figure 1.1 demonstrates the schematic diagram of a stereo vision system. As shown in Fig. 1.1, the image point P (P_L) in the 3-D world along with the focal point of two lenses O_L and O_R form the **epipolar plane**. The line intersecting this plane with the right-hand camera is called the **epipolar line**. Here, if a correspondence can be found between the two images points P_L and P_R, then the 3-D reconstruction can be achieved by triangulation, provided that the position of projection centers, the effective focal length, and the orientation of axes is known. According to the constraint of epipolar geometry, all corresponding possible points for P_L on right hand camera should lie on the epipolar line. Hence the point correspondence searching problem becomes 1-D, this allows better accuracy as well more efficiency for the 3-D reconstruction process.

The stereo vision has a few merits which include:

- The setup is simple.
- This method can achieve high speed measurements given that cameras with high image acquisitions rates are available.

However, there are some weaknesses associated with this process as well.

- This method is computationally expensive (mainly for finding the correspondence).

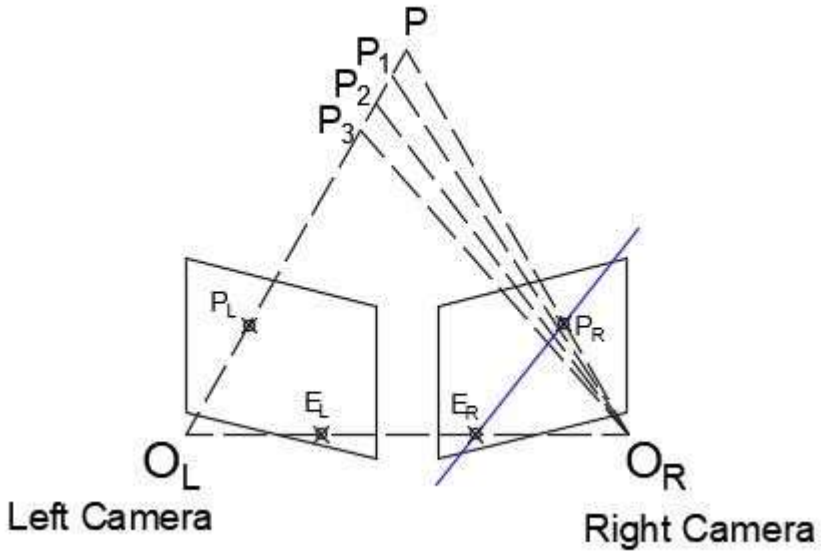

Figure 1.1 Illustration of principle of Stereo Vision system

- The correspondence detection might fail in cases where there are regions of uniform or repetitive textures.

1.2.2.4 Structured Light

The structured light technique is similar to stereo vision technique, except for the fact that there is only one camera involved while the other camera is replaced by a projector. This method is used to ease the correspondence problem in stereo vision technique (Salvi et al., 2004). In this case the projector projects preloaded patterns on the object rather than relying on natural texture (Geng, 2011).

Figure 1.2 illustrates the principle of the structured light technique. Figure 1.2(a) shows a schematic diagram of the structured light technique. Here **A** represents a projector pixel, **D**

represents a camera pixel and the **B** is the object point being imaged. The projector projects various fringe patterns (which are preloaded) on the object. Since the object usu-

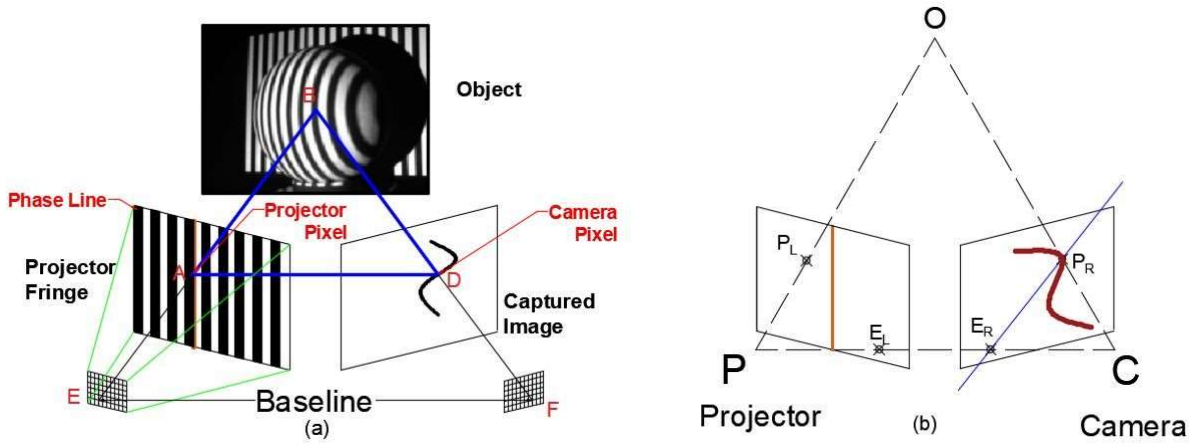

(a) (b)

Figure 1.2 Concept of structured light technique. (a) Schematic diagram explaining the principle of structured light technique; (b) correspondence determination by finding the intersection point between phase line and epipolar line.

ally has curved surfaces; the projected fringe patterns will get distorted by the surface which is then captured by the camera. While Fig. 1.2(b) illustrates the determination of the correspondence between camera and projector points with the constraints of epipolar geometry and phase lines. Given that the method also uses epipolar geometry to compute the 3-D world coordinate through triangulation, it requires at least 1-D correspondence which can be achieved by various ways like:

a. 2D pseudorandom codifications

In this technique, a unique pattern is required with variations in both u and v directions. This can be done by generating a pseudorandom pattern or directly using the natural speckle pattern of a laser source (Payeur and Desjardins, 2009; Song and Chung, 2008). In this case, a $n_1 \times n_2$ array is encoded using a pseudorandom sequence

so that any $k_1 \times k_2$ kernel is unique within the array. The polynomial modulo n^2 method is used in order to encode the array.

This model can be illustrated as (Bell et al., 2016):

$$2_n - 1 = 2_{k1k2} - 1 \tag{1.2}$$

$$n_1 = 2_{k1} - 1 \tag{1.3}$$

$$n^2 = 2^n - \frac{1}{n_1} \tag{1.4}$$

An example of generated pseudo random pattern is shown in Fig. 1.3. This is a simple model which is easy to implement but on the other hand:

- It could be sensitive to noise.
- It is difficult to achieve a high spatial resolution given that each unique feature coding takes many projector pixels.

However, given the aforementioned epipolar geometry constraints as shown in Fig. 1.2(b), only 1-D correspondence is needed. Therefore, the patterns can be designed which vary in one direction only (Pages et al., 2004, 2005).

Figure 1.3 An example of pseudo random pattern.

b. Binary coding method

This is one of the simplest method for 1-D correspondence detection as it uses only two binary intensity stripes with each unit assigned to a value (either 0 or 1). Here, basically a sequence of black and white patterns are projected by the projector on the object to

be scanned and the camera captures the pictures of the distorted patterns. Once the images are captured, then the camera gray scale images are also binarized resulting into each pixel having a codeword of either 0 or 1. Figure 1.4 shows an example of a sequentially projected binary patterns and the associated assigned codeword. This codeword will serve as cues for 1-D correspondence detection. The 3-D coordinates can then be recovered by triangulation between the projector stripes, camera points and the scanned object point.

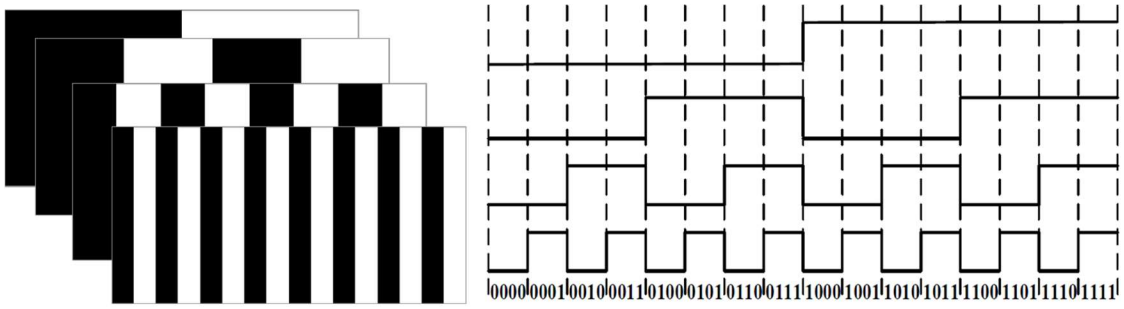

Figure 1.4 An example set of patterns and associated codifications of the binary coding method.

There are various advantages of using binary coding method. First of all, it is very simple and robust as only two states (i.e. only 0 and 1) are used at any given point. Conversely, the limitations of this method are:

- The individual pixels within each black or white stripe cannot be differentiated.
- n patterns are required to encode 2^n pixels, meaning that the number of patterns required can be quite big if a high-resolution scene is to be coded.

c. N-ary codification method

The N-ary codification method (Chazan and Kiryati, 1995) is similar to binary codification method. This method uses multiple intensity values instead of binary

intensities to encode the scene. N-ary codification method uses any subset of intensities from 0 to 255. The intensity ratio calculation is used to estimate the codeword of the pixel in this case. Figure 1.5(a) - 1.5(b) show an example N-ary pattern and an associated cross-section demonstrating multiple gray levels. The advantage of this method is that by increasing the number of gray levels, the number of patterns needed is reduced compared to the binary codification method. Therefore, the potential sensing speed is increased. But in doing so, the robustness is compromised. This method is less robust towards noise than the binary codification method as accuracy on intensity acquisition becomes critical. The other disadvantage of this process being that, it is very sensitive to focus level of the camera and the projector.

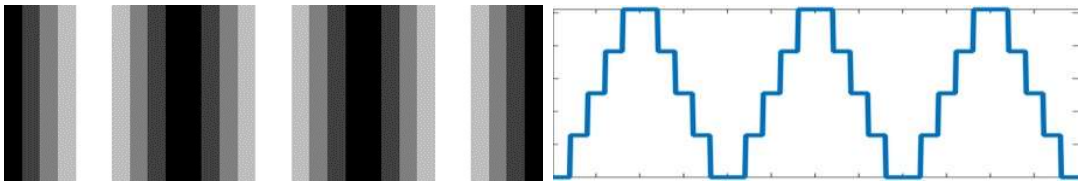

(a) (b)

Figure 1.5 Concept of N-ary codification. (a) An example N-ary pattern; (b) a cross–section of (a) showing multiple gray levels.

d. Digital fringe projection (DFP)

In the DFP technique, the sinusoid projections are used to address the shortcomings of the binary and N-ary codification methods. This means that continuously varying patterns are projected on the object rather than binary or multi-gray-level patterns. This is another form of structured light method like binary and N-ary codification technique discussed in the previous sections. In fact, the idea of DFP came from the fact that many pattern projections (e.g. binary stripes, N-array) will look like sinusoidal if sufficiently blurred by the defocusing. Figure 1.6(a) - 1.6(b) show the corresponding

pattern and cross-section of Fig. 1.5(a) - 1.5(b) after sufficient amount of defocusing. One can clearly see that sinusoidal profiles are produced once the pattern is defocused, which is then taken advantage of by the DFP technique. The DFP technique uses phase instead of intensity for coding the object. This technique is superior than the structured light techniques mentioned above in various ways:

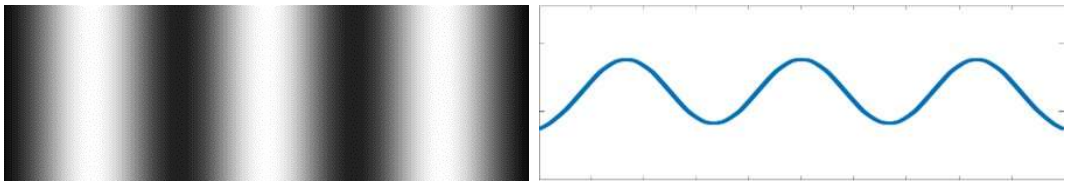

(a) (b)

Figure 1.6 Concept of sinusoidal codification. (a) A example sinusoidal pattern; (b) a cross-section of (a) showing the sinusoidal profile.

- Since the intensity varies from one point to another throughout the image, pixellevel resolution is possible. Hence the determination of correspondence between the camera and the projector can be made more precisely.
- This method is comparatively more robust to geometric and surface texture variation as this method uses phase instead of intensity.

There are various methods to generate sinusoidal fringe patterns. The laser interference can be used to generate these patterns, but laser usually tends to have some speckle noise. This can degrade the accuracy of the measurement. The DFP technique uses computer generated digital sinusoidal fringe patterns. Some popular methods such as the Fourier transform profilometry (FTP) (Takeda and Mutoh, 1983) or the phaseshifting techniques (Srinivasan et al., 1984; Huang and Zhang, 2006; Malacara, 2007) can be used for phase recovery.

As mentioned above, there are various advantages of using DFP, hence it is extensively used (Geng, 2011). However, there are a couple of drawbacks of the technique that cannot be ignored:

- First of all, the measurement speed has a bottleneck (e.g. 120 Hz). This is because the sinusoidal patterns are in 8-bit form, so the measurement speed is restricted to 8-bit refreshing speed of the projector.
- The non-linear gamma effect is very evident in the commercial projectors which was designed to accommodate human vision. This leads to error in calculated phase map.

1.2.2.5 Binary defocusing technique

As mentioned in the above section, the major limitation of DFP technique is its speed constraint as it uses 8-bit fringe patterns. Hence it is not suitable for high speed applications. This led to the introduction of binary defocusing method proposed by Lei and Zhang (Lei and Zhang, 2009). This method allows faster 3-D imaging rate as it uses 1-bit patterns, since using 1-bit patterns rather than 8-bit patterns allows faster image transfer rate. This method is used along with the digital light processing (DLP) technique for high speed applications. The DLP platform produced by Texas Instruments allowed the rate at which the binary images can be switched with a rate about tens of kHz (Hornbeck, 1999).

The working principle of DLP technique is illustrated in Fig. 1.8. The DLP technique uses digital micro-mirror device (DMD) to modulate light digitally with an array of micro mirrors which in turn corresponds to pixels in projected image. There are micro-mirrors which are either tilted towards or away from the light source with the help of a tiny electrode beneath

the DMD cell. As shown in Fig. 1.7, the signal forces the mirror to switch 'ON' (i.e. $+\theta_L$) or 'OFF' (i.e. $-\theta_L$). Here the brightness of a pixel is controlled by the amount of time that the

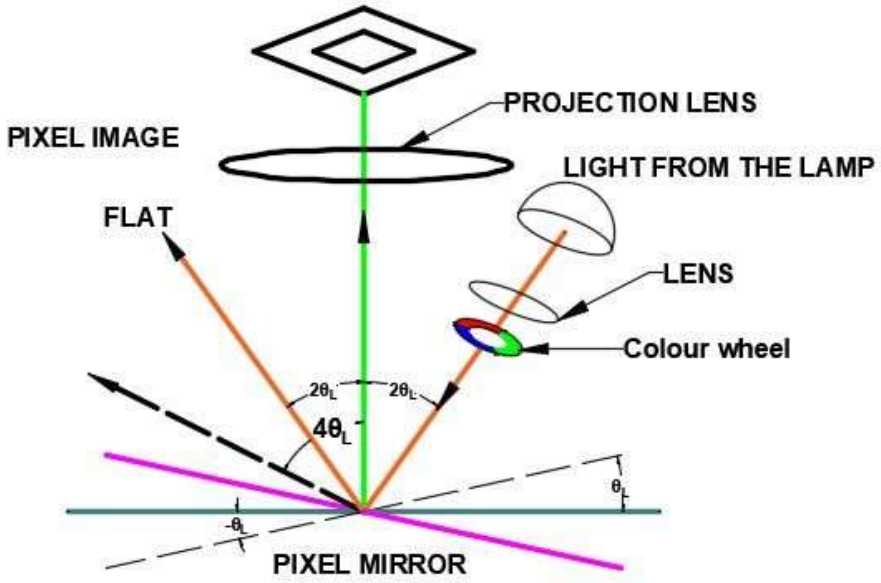

Figure 1.7 Working principle of Digital Light Processing method

mirror is switched on as the DLP projector produces grayscale values by time integration (Hornbeck, 1997). Hence, a gray scale value will be 255 if the mirror is switched on all the time. Conversely, if the mirror is turned off all the time, the corresponding value will be 0. Therefore, the whole projection cycle is not required if the projector is supplied with either 0 or 255 grayscale values only (working as solid states). That is why, this technology is suitable for high speed applications.

As discussed in the earlier sections, if the binary patterns are sufficiently defocused, then the resultant pattern will be similar to sinusoidal patterns. However, one has to keep in mind that the defocusing should be properly controlled. As can be seen in Fig. 1.8, if the pattern is not defocused enough, the pattern will be basically retain a binary structure (see the first

image in Fig. 1.8), but too much defocussing will lead to diminished patterns (i.e. low fringe quality) which corresponds to the last image in Fig. 1.8. Therefore, neither too focused nor too defocused patterns are desirable as they could introduce periodical phase errors or have low signal-to-noise ratio.

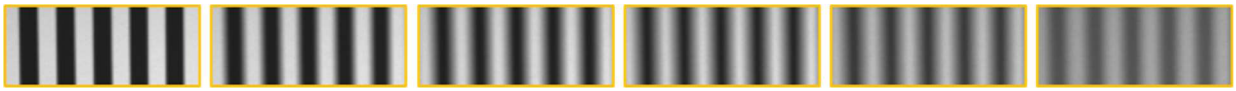

Figure 1.8 Binary Projection at different defocusing levels with the first image being in-focus. The sinusoidal structures appear in the mid-level of defocusing.

1.3 Objective

Although using binary patterns has the constraint of proper defocusing control, it still has many advantages over sinusoidal patterns. First and foremost, they are 1 bit patterns, hence it is more suitable for high speed applications. Moreover, since the patterns only include two grayscale values (0 and 255), the nonlinear gamma problem associated with 8-bit patterns becomes trivial. This thesis research aims at addressing the aforementioned limitation of the binary defocusing method. Specifically, we propose a binarized dual phase shifting (BDPS) method and a Hilbert binarized dual phase shifting (HBDPS) method to tackle the phase errors of the binary defocusing method when the projector is not sufficiently defocused. The detailed discussion on both methods is provided in Chapter 3 of this thesis.

1.4 Organization

The organization of the thesis is illustrated as follows:

- Chapter 2 introduces the basic principle of the DFP technique along with three-step phase shifting algorithm. Then, the principles of binary defocusing, system calibration and 3-D reconstruction will also be discussed in this chapter.
- Chapter 3 introduces the details of proposed BDPS and HBDPS methods for highquality 3D shape measurement.
- Finally, Chapter 4 summarizes the thesis and some future scope of work.

CHAPTER 2. BASIS OF 3-D SHAPE MEASUREMENT

In the previous chapter, we introduced the motivation of this thesis study, an overview of 3-D shape measurement technologies, and the organization of this thesis. In this chapter, the fundamentals of 3-D shape measurement using the digital fringe projection (DFP) will be introduced, including the basics of DFP technique, the theory of phase shifting technique, the details of pinhole model and system calibration, as well as 3-D reconstruction.

2.1 Digital Fringe Projection (DFP)

In the DFP technique, sinusoidal patterns are projected by the projector as opposed to binary or N-ary codification techniques discussed in the previous chapter. In fact, many different types of patterns (e.g. binary stripes, N-array) will look like sinusoidal patterns when sufficiently blurred.

The DFP technique uses phase instead of intensity for coding the measured scene. For phase retrieval, phase shifting (Srinivasan et al., 1984; Huang and Zhang, 2006; Malacara, 2007) is one of the most widely used approach. For a generic N-step phase shifting, the n-th (n = 1,2,3, 4,....,N) fringe pattern can be represented as

$$I_n(x,y) = I^0(x,y) + I''(x,y)\cos(\varphi + 2n\pi/N) \tag{2.1}$$

Simultaneously solving all n equations, we can retrieve the average intensity:

$$I'(x,y) = \frac{\sum_{n=1}^{N} I_n}{N}; \tag{2.2}$$

The intensity modulation is:

$$I''(x,y) = \frac{\sqrt{(\sum_{n=1}^{N} I_n \cos(2\pi n/N))^2 + (\sum_{n=1}^{N} I_n \sin(2\pi n/N))^2}}{N}; \tag{2.3}$$

The wrapped phase is given by:

$$\phi(x,y) = -\tan^{-1}\left[\frac{\sum_{n=1}^{N} I_n(x,y)\sin(2\pi n/N)}{\sum_{n=1}^{N} I_n(x,y)\cos(2\pi n/N)}\right]. \quad (2.4)$$

Figure 2.1(a) - 2.1(c) show an example of phase shifted patterns when the number of steps N = 3, and Fig. 2.1(d) shows the wrapped phase map obtained from Eq. 2.4. As can be seen in Eq. 2.4, the φ is in an arctangent form which varies between $-\pi$ to π. therefore, there is a phase jump of 2π which can be seen in Fig. 2.1(d). So, in order to get a continuous phase map, the phase needs to be unwrapped using a phase unwrapping algorithm. The phase unwrapping can be done using a spatial (Judge and Bryanston-Cross, 1994; Trouve et al., 1998; Costantini, 1998; Ghiglia and Pritt, 1998) or temporal (Wang and Zhang, 2012a; Ding et al., 2015; Zhang, 2012; Ding et al., 2011) phase unwrapping algorithm. The working principle of such algorithm is to detect the 2π phase jump and then add or subtract the integer multiples of 2π to compensate for it.

$$\Phi(x,y) = \varphi(x,y) \pm k(x,y) \times 2\pi \quad (2.5)$$

Figure 2.1(e) shows the unwrapped phase map. Once the phase is unwrapped and continuous, the 3D geometry can be reconstructed based on calibration, which will be introduced in the next section.

2.2 Calibration

The calibration of all the devices involved (i.e. a camera and a projector) is a key step in order to achieve highly accurate measurement which turns the phase map into 3D geometry. There has been extensive research going on over the years to study calibration of the camera. The calibration of camera for high precision measurement using 3-D targets dates back to 1970s (Duane, 1971; Sobel, 1974). Since then, there has been considerable contributions by various scientists in this field of research. Some later research (Tsai, 1987; Zhang, 2000)

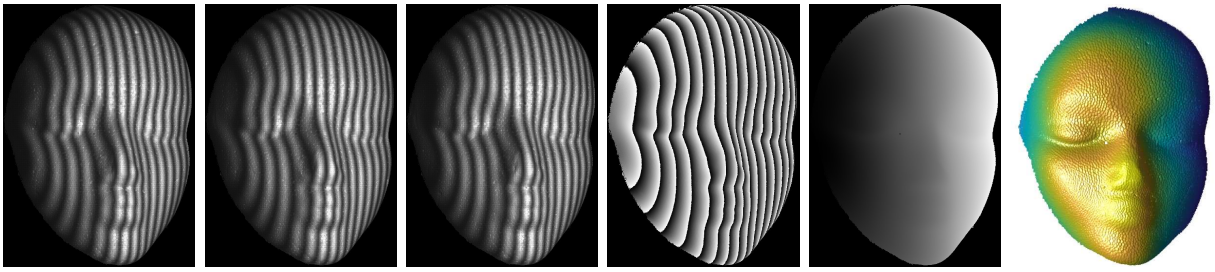

(a) (b) (c) (d) (e) (f)

Figure 2.1 An example procedure for the DFP technique. (a) - (c) Three-step phase shifted patterns; (d) wrapped phase; (e) unwrapped phase; (f) 3D reconstructed geometry.

showed that 2-D calibration targets can be achieved without the requirement of complex 3-D calibration. The recent advancement in the field of calibration techniques has allowed achievement of higher flexibility and accuracy (Lavest et al., 1998; Albarelli et al., 2009; Strobl and Hirzinger, 2011; Huang et al., 2013).

The calibration of structured light system is more complicated as it involves a projector along with a camera. Scientists have proposed various methods to calibrate a structured light system by determination of exact parameters of the system (Hu et al., 2003; Mao et al., 2007). Though successful, the process of finding the exact system parameters can be tedious and time consuming. So in order to save effort and increase flexibility, new calibration methods like reference-plane-based method (Guo et al., 2006; Vo et al., 2012) and "projector as an inverse camera method" (Legarda-Sa´enz et al., 2004; Zhang and Huang, 2006; Li et al., 2008; Yin et al., 2012) were introduced. In this research, we adopted the "projector as an inverse camera method" and the related basic concepts and detailed procedures are introduced below.

2.2.1 Pinhole Model of the Structured Light System

Pinhole model establishes the geometric relationship between the coordinates of a point in 3-D world space with its projection on image planes. Figure 2.2 (Li and Zhang, 2014) demonstrates a pinhole model of the structured light system.

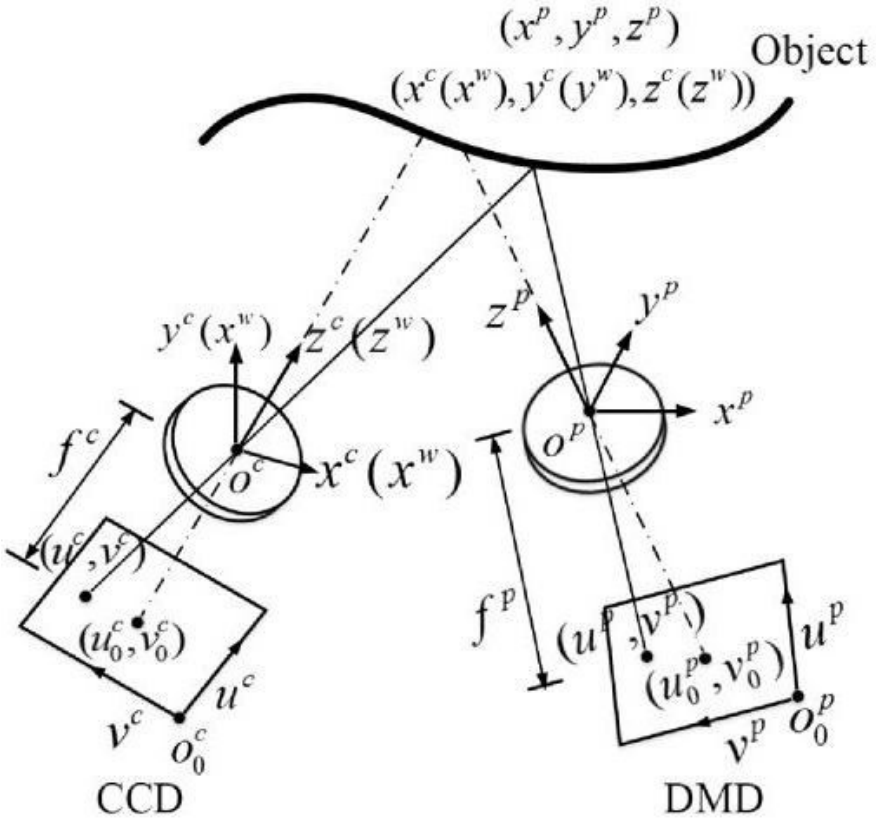

Figure 2.2 Illustration of Pinhole camera model.

The world coordinate system is represented by (o^w,x^w,y^w,z^w) while the (o^c,x^c,y^c,z^c) and (o^p,x^p,y^p,z^p) denote the camera and the projector coordinate systems, respectively. The f^c and f^p are the focal lengths of camera and projector.

The mathematical model can be described as follows:

$$s^c \begin{bmatrix} u^c \\ v^c \\ 1 \end{bmatrix} = A^c \begin{bmatrix} R^c, t^c \end{bmatrix} \begin{bmatrix} x^w \\ y^w \\ z^w \\ 1 \end{bmatrix} \tag{2.6}$$

$$s^p \begin{bmatrix} u^p \\ v^p \\ 1 \end{bmatrix} = A^p \begin{bmatrix} R^p, t^p \end{bmatrix} \begin{bmatrix} x^w \\ y^w \\ z^w \\ 1 \end{bmatrix} \tag{2.7}$$

where,

(o^w,x^w,y^w,z^w) - The world coordinate system .

[R^c,t^c]- Camera extrinsic matrices for rotation and translation respectively.

[R^p,t^p]- Projector extrinsic matrices for rotation and translation respectively.

A^c- Intrinsic matrices of camera which is given by:

$$A^c = \begin{pmatrix} \alpha^c & \gamma^c & u_o^c \\ 0 & \beta^c & u_o^c \\ 0 & 0 & 1 \end{pmatrix} \tag{2.8}$$

A^p- Intrinsic matrices of projector which is given by:

$$A^c = \begin{pmatrix} \alpha^c & \gamma^c & u_o^c \\ 0 & \beta^c & u_o^c \\ 0 & 0 & 1 \end{pmatrix} \tag{2.9}$$

Here, α^c, α^p, β^c and β^p signifies the focal lengths along u^c, u^p, v^c, v^p axes respectively. While γ^c and γ^p are the skew factors of u^c, v^c, u^p, v^p respectively. The f^c and f^p are the focal lengths of camera and projector.

Ideally, the linear relationship described above is sufficient to describe the pinhole lens model. In reality, the camera and the projector can also have nonlinear lens distortion which is given by:

$$Distortion = \begin{bmatrix} k_1 & k_2 & p_1 & p_2 & k_3 \end{bmatrix}^T \tag{2.10}$$

For correction of radial distortion, the following equation can be used:

$$u^0 = u(1 + k_1r^2 + k_2r^4 + k_3r^6) \tag{2.11}$$

$$v^0 = v(1 + k_1r^2 + k_2r^4 + k_3r^6) \tag{2.12}$$

where,

(u,v) and (u^0,v^0) are the camera or projector pixel point coordinate before and after correction. $r = \sqrt{u^2 + v^2}$ is the tangential distortion can be corrected by:

$$u^0 = u + [2p_1uv + p_2(r^2 + 2u^2)] \tag{2.13}$$

$$v^0 = v + [2p_2uv + p_1(r^2 + 2v^2)] \tag{2.14}$$

Furthermore, a simplified model of the structured light system can be obtained by coinciding the world coordinate system with camera coordinate system which is given by:

$$R_3 = E_3, \qquad t^c = 0 \tag{2.15}$$

$$R^p = R, \qquad t^p = t \tag{2.16}$$

Here, E_3 is the 3 × 3 identity matrix. R and t are the affine transformation parameters that describe the transformation from the camera lens coordinate system to projector lens coordinate system.

2.2.2 Calibration Procedure

The system (i.e. the camera and the projector) is calibrated in order to determine the intrinsic and the extrinsic parameters discussed above. The camera can be calibrated using the OpenCV camera calibration toolbox. Figure 2.3 illustrates a sample calibration board for camera calibration. Here the circles are extracted as feature points. The projector calibration is usually done by one-to-one phase mapping between the camera and the projector sensor.

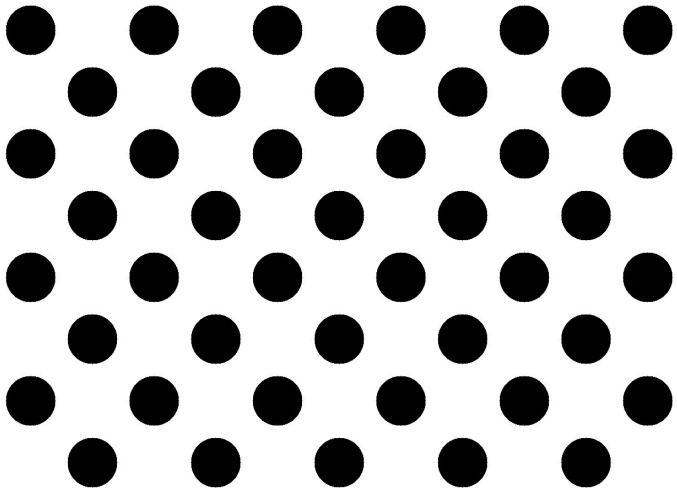

Figure 2.3 An example of calibration board.

The detailed procedures are as follows:

- **Step 1: Image capture** - In order to calibrate the system, both an actual image of the target as well as the fringe images are required. A sequence of horizontal and vertical phase shifting fringe patterns are projected and captured for absolute phase recovery.

- **Step 2: Intrinsic calibration of camera** - The OpenCV camera calibration tool is used to find the circle centers, intrinsic parameters and the lens distortion parameters of the camera. This step needs to use the actual image of the target at different poses and is done by the OpenCV function *cv:calibrateCamera*.

- **Step 3: Circle center determination for the projector** - Once the pixel coordinate (u^c,v^c) of the circle center points for the camera target images are determined, then the projector circle centers can be determined as well. To start with, one needs to get the absolute horizontal and vertical phase maps Φ_{ha} and Φ_{va} using the phase shifting algorithm. Then, the circle centers for the projector (u^c,v^c) can be determined by a linear 2-D mapping:

$$v^p = \Phi^c{}_{\mathrm{va}}(u^c, v^c) \times \frac{T}{2\pi} \tag{2.17}$$

$$u^p = \Phi^c{}_{\mathrm{ha}}(u^c, v^c) \times \frac{T}{2\pi} \tag{2.18}$$

where, u^p,v^p= mapping points for the projector. u^c,v^c= mapping points for camera.

T = Fringe period for the narrowest fringe pattern.

$\Phi^c{}_{\mathrm{ha}}$= Absolute horizontal gradient phase map.

$\Phi^c{}_{\mathrm{va}}$= Absolute vertical gradient phase map.

- **Step 4: Intrinsic Calibration of projector** - Once the pixel coordinate (u^p,v^p) of the circle center points for the projector target images are determined, then the OpenCV toolbox can also be used to determine the intrinsic parameters of the projector. This step is also done by using the OpenCV function *cv:calibrateCamera*.

- **Step 5: Extrinsic Calibration** - The extrinsic calibration can be done once the intrinsic parameters are known. The OpenCV stereo calibration toolbox (*cv:stereoCalibrate*) can be used to determine the extrinsic matrix (i.e. [R,t]).

2.3 3-D Reconstruction

After calibration, we have obtained the previously unknown parameters in the system pinhole model.

In the simplified pinhole model, we have made $R_3 = E_3$, $t^c = 0$ and $R^p = R$, $t^p = t$.

By simplifying both the camera and projector projection matrices, we get:

$$M^c = A^c[E_3, 0] \tag{2.19}$$

$$M^p = A^p[R, t] \tag{2.20}$$

Where,

M^c- The combined camera projection matrix.

M^p- The combined projector projection matrix.

A^c- The intrinsic matrix of camera.

A^p- The intrinsic matrix of projector.

$[R,t]$ - The translation and rotation from the camera coordinate system to the projector coordinate system.

The matrices can be determined after the calibration of the system. Therefore, from Eq. 2.6 - 2.7 and Eq. 2.19 - 2.20, we get:

$$\begin{bmatrix} x^w \\ y^w \\ z^w \end{bmatrix} = \begin{bmatrix} m^c_{11} - u^c m^c_{31} & m^c_{12} - u^c m^c_{32} & m^c_{13} - u^c m^c_{33} \\ m^c_{21} - v^c m^c_{31} & m^c_{22} - v^c m^c_{32} & m^c_{23} - v^c m^c_{33} \\ m^p_{11} - u^p m^p_{31} & m^p_{12} - u^p m^p_{32} & m^p_{13} - u^p m^p_{33} \end{bmatrix}^{-1} \begin{bmatrix} u^c m^c_{34} - m^c_{14} \\ v^c m^c_{34} - m^c_{24} \\ u^p m^p_{34} - m^p_{14} \end{bmatrix} \tag{2.21}$$

$m^c_{i,j}$ - The camera matrix element at $i^{th.}$ row and $j^{th.}$ column. $m^p_{i,j}$ -

The projector matrix element at $i^{th.}$ row and $j^{th.}$ column.

Eq 2.21 basically describes the 3-D reconstruction using the calibration parameters. Using this equation, each camera pixel (u^c,v^c) will result in a 3-D coordinate (x^w,y^w,z^w).

2.3.1 Summary

This chapter introduced the DFP technique along with the concept of phase shifting algorithm and phase recovery. Then basic concepts of pinhole model, the detailed procedures for system calibration as well as 3-D reconstruction are also introduced. The next chapter will introduce the proposed binarized dual phase shifting (BDPS) method and Hilbert binarized dual phase shifting (HBDPS) method that are used to perform high-quality 3-D shape measurement while preserving the high-speed advantage of binary patterns.

CHAPTER 3. BINARIZED DUAL PHASE-SHIFTING METHOD FOR HIGH QUALITY 3D SHAPE MEASUREMENT

3.1 Introduction

Three-dimensional (3D) shape measurement plays a significant role in many areas ranging from manufacturing to medicine. Numerous techniques have been developed including Moire, holography, and fringe projection. Among these methods, the digital fringe projection technique has been extensively studied and widely applied due to its simple setup, automatic data processing, high-speed and high-resolution measurement capabilities (Gorthi and Rastogi, 2010)

For high-speed and high-accuracy 3D shape measurement, it has been demonstrated that using 1-bit binary patterns is advantageous over 8-bit sinusoidal phase-shifted fringe patterns especially on the digital-light-processing (DLP) projection platform (Zhang et al., 2010). By properly defocusing the projector for specific square binary patterns (Lei and Zhang, 2009), researchers have achieved the speed breakthroughs for high-accuracy 3D shape measurement. However, such a method requires the projector to be properly defocused in order to suppress the high-order harmonics, thus its measurement depth range is severely limited. In the last few years, lots of research have been conducted to alleviate this problem. Several different pulse width modulation (PWM) techniques are introduced to shift or eliminate the undesired high-order harmonics (Ayubi et al., 2010; Wang and Zhang, 2010; Zuo et al., 2012), and thus the phase quality can be effectively improved. However, due to their one-dimensional (1D) modulation nature, such methods work well only when the fringe period is relatively narrow. To further improve this, 2D modulation methods such as area-modulation and dithering techniques are proposed for better approximation of sinusoidal patterns (Lohry and Zhang, 2012; Wang and Zhang, 2012b). Such methods generally require

a time-consuming optimization process to find the best binarized patterns (Dai et al., 2014; Dai and Zhang, 2013).

Another kind of approach is to utilize the characteristics of the phase distribution for error compensation. Xu et al. (Xu et al., 2011) established a mathematical phase error function in terms of the wrapped phase and depth z, and used the model to compensate the phase error in the calibration volume. This method requires careful and accurate calibration in order to achieve high-accuracy measurement. Instead, Zhang (Zhang, 2011) proposed a simple and effective error compensation strategy called dual phase-shifting algorithm (DPS). Given that the phase error has an obvious 6× periodicity, this method projects an additional set of fringe patterns with a shift of 1/12 period (or $\pi/6$) compared to the original patterns, and performs error reduction by averaging the two-phase maps. However, as introduced, the DPS method requires two sets of phase shifted fringe patterns, which is not desirable in high-speed applications.

In this paper, a binarized dual phase-shifting algorithm (BDPS) is proposed to generate high-quality phase using just three phase-shifted binary patterns. By combining the two sets of $\pi/6$ shifted square binary patterns, a single set of phase shifted patterns with three gray levels is obtained, which is further binarized by utilizing 2D modulation to preserve the speed advantage of using binary patterns. Besides, to further reduce the phase error, Hilbert binarized dual phase-shifting algorithm (HBDPS) is proposed by applying the Hilbert transform for error compensation. Both simulations and experiments are conducted to verify the effectiveness of the proposed methods.

3.2 Principle

3.2.1 Single Phase-shifting algorithm (SPS)

Phase-shifting methods are widely used in optical metrology because of their speed and accuracy (Malacara, 2007). If a multi-step phase-shifting algorithm with a phase shift of δ_n is adopted, the intensity distributions for the ideal sinusoidal fringes can be described as

$$I_n(x,y) = A(x,y) + B(x,y)\cos(\Phi + \delta_n), (n = 1,2,3,...,N), \tag{3.1}$$

where $A(x,y)$ is the average intensity, $B(x,y)$ the intensity modulation, and $\Phi(x,y)$ the phase to be solved for. The wrapped phase can be calculated from the following least-square algorithm,

$$\phi(x,y) = -\tan^{-1}\left[\frac{\sum_{n=1}^{N} I_n(x,y)\sin\delta_n}{\sum_{n=1}^{N} I_n(x,y)\cos\delta_n}\right]. \tag{3.2}$$

The arctangent function will produce a value ranging $[-\pi, +\pi)$ with 2π discontinuities. In order to remove the 2π discontinuities and obtain the absolute phase map, spatial or temporal phase unwrapping algorithms are generally required. In this research, we used an enhanced two-wavelength phase shifting method (Hyun and Zhang, 2016) for temporal phase unwrapping. However, if the phase shifting technique is adopted with binary patterns, a crucial limitation is that the fringe patterns will not be ideally sinusoidal when the projector is not properly defocused, which is actually very common considering the measurement range.

Therefore, the unsuppressed high order harmonics would introduce phase error.

3.2.2 Dual phase-shifting algorithm (DPS)

With undesired high-order harmonics, the square binary fringe patterns can be described as

$$I_n^C(x,y) = A(x,y) + \sum_{k=1}^{\infty} B_k(x,y)cos[k(\phi(x,y) + \delta_n)] \tag{3.3}$$

The phase error due to the undesired harmonics for a N-step phase shifting method is as follows:

$$\Delta\phi_N = \tan^{-1}\left[\frac{\sum_{m=1}^{\infty}(B_{mN+1} - B_{mN-1})\sin(mN\phi)}{1+\sum_{m=1}^{\infty}(B_{mN+1} + B_{mN-1})\cos(mN\phi)}\right]. \tag{3.4}$$

Generally, a three-step phase-shifting algorithm, which requires the least steps of phase shifts, is preferred when requiring high measurement speeds. Thus, in this paper, all analysis is based on the three-step phase-shifting algorithm while the technology should also be adaptable for multi-step algorithms. For a square binary pattern, it is well known that only $(2k + 1)^{th}$ order harmonics exist. A simulation similar to Ref. (Zhang, 2011) was conducted to demonstrate the phase errors induced by different harmonics.

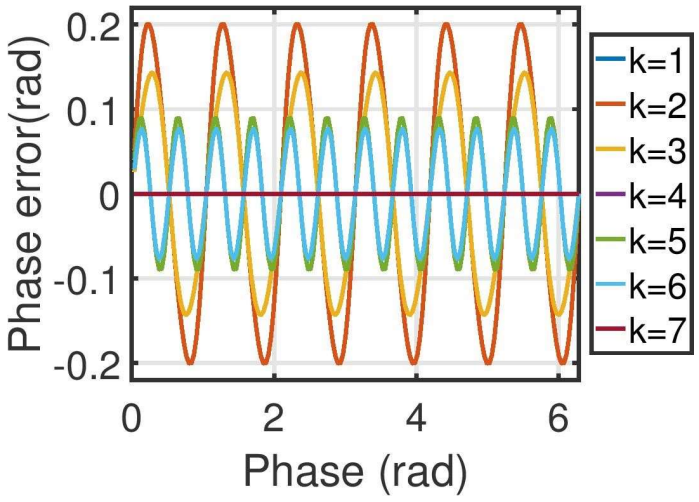

Figure 3.1 Phase errors induced by $(2k + 1)^{th}$ (k = 1,2,3...) order harmonics.

Figure 3.1 shows the phase errors from different harmonics if a three-step phase-shifting algorithm is utilized. It shows that the third (k = 1, $2k$ +1 = 3), ninth (k = 4, $2k$ +1 = 9), and fifteenth (k = 7, $2k$ + 1 = 15) order harmonics will not bring phase error because an equal phase-shift of $2\pi/3$ is utilized between patterns. It also indicates that the low frequency harmonics (i.e. less than eleventh (k = 5) order) introduces 6× phase error, which is consistent with the theoretical analysis. As introduced by Zhang (Zhang, 2011), if another phase map with a phase-shift of 1/12 period (or $\pi/6$) is obtained, it can be used to compensate for this error by averaging it with the original phase map. Given the fact that two sets of fringe patterns are used in such technique, it is called the dual three-step phase-shifting (DPS) method.

3.2.3 Binarized dual phase-shifting algorithm (BDPS)

For the DPS method, in order to compensate for the dominant 6× phase error, two sets of phase shifted patterns are required and thus the measurement speed would be much slower. For example, for a binary three-step phase-shifting algorithm, the DPS method needs at least six fringe patterns plus additional patterns for temporal phase unwrapping as reported in Ref. (Zhang, 2011). In this paper, a binarized dual three-step phase-shifting algorithm (BDPS) is proposed to overcome this problem. The basic idea is to incorporate the two sets of square binary phase-shifting patterns into one pattern set with three gray levels, which is further binarized by utilizing 2D modulation. Therefore, the BDPS method can realize the error compensation for binary defocusing technique while not increasing the total number of patterns or the total number of bits.

Figure 3.2 shows the principle of BDPS method. Figure 3.2(a) shows the cross sections of the original square binary pattern with a fringe period of T = 36 pixels and the shifted square pattern with a shift of 1/12 period (or 3 pixels). By averaging the two square binary patterns,

a new structure with three gray levels is obtained as shown in Fig. 3.2(b). The original square binary pattern is shown in Fig. 3.2(c). To generate the introduced middle gray level as shown in Fig. 3.2(b) with only 1-bit binary (0 or 255) intensities, a binary 2D modulation method is employed. As shown in Fig. 3.2(d), the supposed middle gray level pixels are approximated with evenly distributed black-white structures.

Considering the characters of the 2D modulation, a slight defocusing effect could make the BDPS pattern close to the designed three-gray-level structure, and thus finally realizes the error reduction.

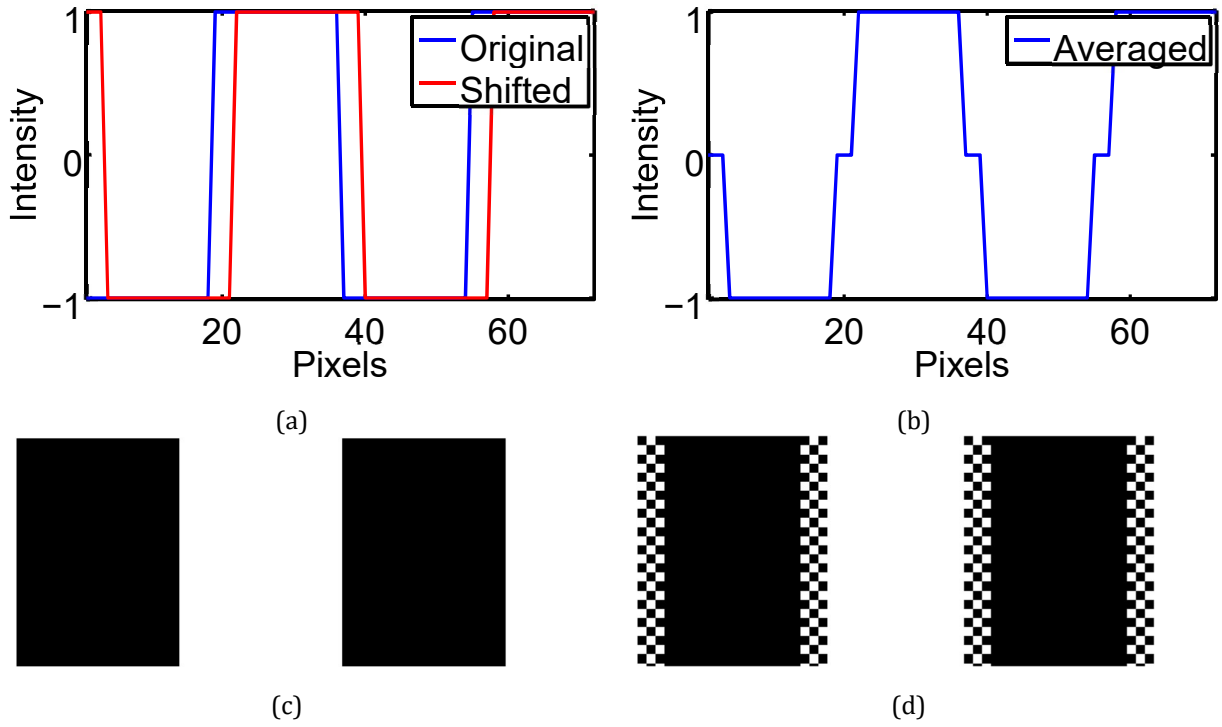

Figure 3.2 Steps to generate a BDPS pattern. (a) An overlay of the cross-sections of the original and the $\pi/6$ shifted square binary pattern; (b) the average of the pattern cross-sections in (a) exhibiting three gray levels; (c) - (d) the original square binary pattern and the BDPS pattern, the BDPS pattern is generated by binarizing the middle gray level shown in (b).

3.2.4 Hilbert binarized dual phase-shifting algorithm (HBDPS)

For further error reduction, we also propose a Hilbert binarized dual phase-shifting algorithm (HBDPS). The theoretical foundation is explained as follows: by applying the Hilbert transform, a phase shift of $\pi/2$ will be applied to all the phase shifted fringe patterns.

$$I_n^H(x,y) = \mathbf{H}[I_n(x,y)] = -B(x,y)sin[\phi(x,y) + \delta_n] \tag{3.5}$$

Based on the Hilbert transformed phase-shifting patterns, an additional Hilbert phase can be obtained as

$$\phi^H(x,y) = \tan^{-1}\left[\frac{\sum_{n=1}^{N} I_n^H(x,y)\cos\delta_n}{\sum_{n=1}^{N} I_n^H(x,y)\sin\delta_n}\right]. \tag{3.6}$$

Due to the additional phase shift of $\pi/2$, the phase errors of the original phase $\varphi(x,y)$ and the Hilbert phase $\varphi^H(x,y)$ have opposite distributional tendencies (Cai et al., 2015). By averaging the two phases, the final phase map can be calculated and the phase errors can be further reduced.

$$\varphi^f(x,y) = \varphi(x,y)/2 + \varphi^H(x,y)/2. \tag{3.7}$$

To compare the performances of SPS, BDPS and HBDPS methods, we applied $n \times n$ pixel Gaussian filters with a standard deviation of $n/3$, here n = 3,5,7,...,15,17,19. These filter sizes essentially emulates the varying amounts of defocusing levels. By employing a three-step phase-shifting algorithm, we computed the phase root-mean-square (rms) error under each filter size. Figure 3.3(a) shows the cross sections of the phase error maps for all three methods when the filter size is n = 3. For a more extensive testing, we also plotted the phase rms error as a function of filter size, which is shown in Fig 3.3(b). It is observed that the BDPS method can effectively reduce the dominant phase errors especially when the amount of defocusing is small, while the HBDPS is even slightly better than the BDPS under such

scenario. The difference between the three methods will be reduced when a sufficient amount of defocusing is applied.

3.3 Experiments

Apart from the simulation, we also evaluated the performance of our proposed methods through experiments. The experimental system includes a CMOS camera (model: FLIR Grasshopper3 GS3-U3-41C6C-C) that is attached with a 12 mm focal length lens (model: Computar M1214-MP2), and a projector with DLP development kit (model: Texas Instru-

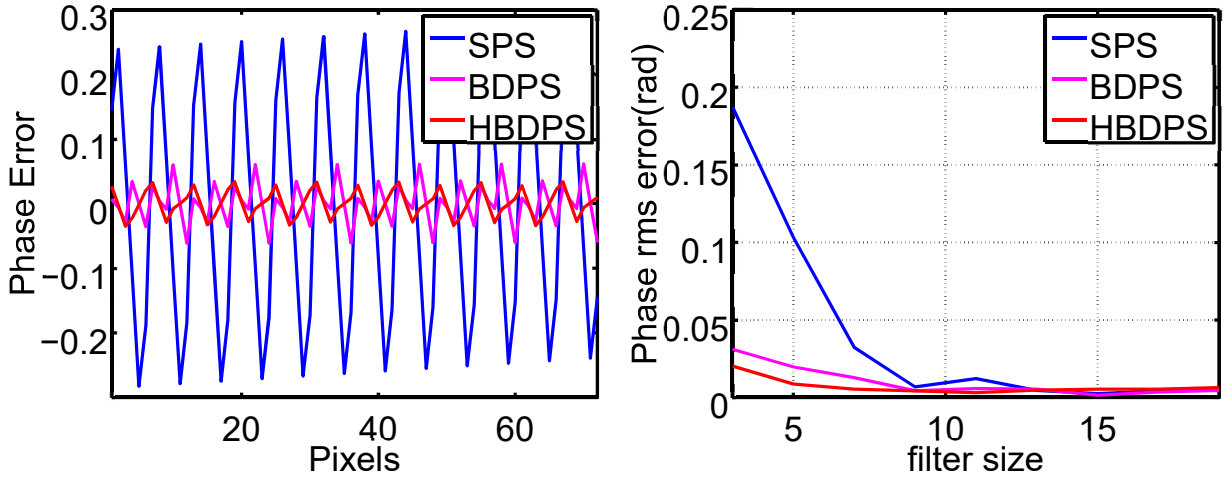

(a) (b)

Figure 3.3 A simulation conducted to compare the performance of SPS, BDPS and HBDPS methods under different sizes of Gaussian smoothing filters (to emulate different projector defocusing levels). (a) The comparison of a cross section of the phase error maps when a small (3×3) Gaussian filter is applied; (b) a more thorough evaluation by comparing the rms errors at different sizes of Gaussian smoothing filters.

ment Lightcrafter 4500). The camera resolution was set as 1280 × 960 pixels and the DLP projector has a 912 × 1140 pixels native resolution.

A flat white paper was first measured to conduct quantitative evaluation. To perform the comparison between all three methods, we captured six binary patterns with a fringe period of T = 36 pixels, including a set of three-step phase shifted square binary patterns and BDPS patterns, respectively. We compared the measured phase quality by taking the difference between the measured phase Φ and a reference phase Φ^r. The reference phase map Φ^r was generated by employing a set of 18-step phase-shifted fringe patterns with a fringe period of T^r = 18 pixels, and then smoothed out by a Gaussian filter with a size of

21 × 21 pixels. To compute the phase error, we took the difference between the measured phase map Φ (fringe period T) and the reference phase map Φ^r (fringe period T^r) as

$$\Phi_{err} = \Phi - \Phi^r \times \frac{T^r}{T}. \tag{3.8}$$

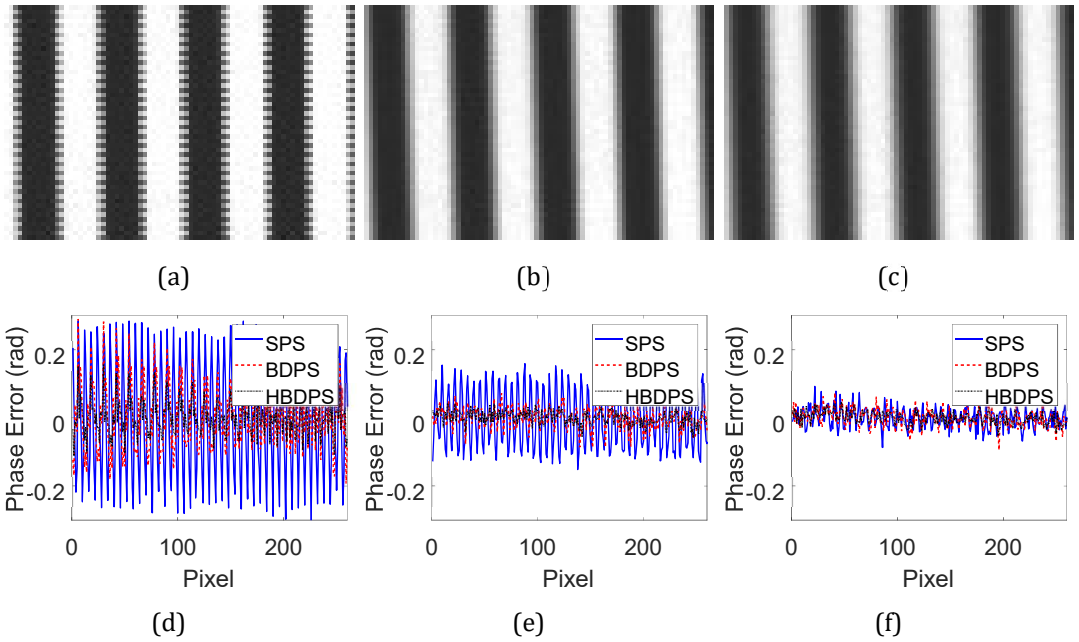

Figure 3.4 Phase error evaluation through measurement of a white planar surface. (a) - (c) Fringe images corresponding different projector defocusing degrees (in-focus, slightly defocused, significantly defocused); (e) - (h) corresponding phase errors plots. The RMS errors of (e) are 0.172 rad (SPS), 0.092 rad (BDPS) and 0.046 rad (HBDPS), respectively; the RMS errors of (f), the RMS errors are 0.088 rad (SPS), 0.031 rad (BDPS) and 0.019 rad (HBDPS), respectively; the RMS errors of (g), the RMS errors are 0.030 rad (SPS), 0.026 rad (BDPS) and 0.018 rad (HBDPS), respectively.

To verify our simulation results, we tested the performance of SPS, BDPS and HBDPS under three different defocusing levels. Figure 3.4(a) - 3.4(c) show a representative captured fringe image when the projector is in-focus, slightly defocused and sufficiently defocused, respectively. Figure 3.4(d) - 3.4(f) show the corresponding comparison of phase errors for all three methods under the three defocusing levels. From the results, we can see that when the projector is in-focus, the phase error of SPS is approximately two times the BDPS phase error, and four times the HBDPS phase error. When the projector is slightly defocused, the difference between BDPS and HBDPS decreases, yet both of them still have an apparent

better performance than the conventional SPS. When the projector is sufficiently defocused, the performance of all three methods become similar since the projector defocusing itself will suppress most of the high order harmonics, yet BDPS and HBDPS still slightly outperform the conventional SPS. This experimental result agrees well with the simulation result shown in Fig. 3.3, which further proves the effectiveness of our proposed BDPS and HBDPS methods.

To qualitatively demonstrate the performance enhancement of our proposed BDPS and HBDPS over the conventional SPS method, we also conducted a similar experiment by measuring the 3D shape of a sculpture surface with geometric variations. The results of 3D reconstruction are shown in Fig. 3.5. The first column shows a representative captured fringe image with the aforementioned three increasing levels of projector defocusing. The second to the last column respectively show the 3D reconstructed geometries using the SPS, BDPS and HBDPS methods correspondingly under the three different projector defocusing levels. Again, the results show that when the projector is in-focus or slightly defocused, the harmonic errors are quite evident on the SPS results, yet such errors are less apparent on the BDPS results and is further alleviated on the HBDPS results. When the projector is significantly out-of-focus, the performance difference between all three methods are significantly reduced, while BDPS and HBDPS still have a slightly better performance than SPS. This qualitative experimental evaluation agrees well with both the simulation and the previous quantitative experimental results, which again validates the success of our proposed BDPS and HBDPS methods.

3.4 Summary

In this research, we propose a binarized dual phase-shifting method for high-quality 3D shape measurement with only three 1-bit binary patterns. Inspired by the dual phaseshifting method which compensates the harmonic phase errors with an additional set of three square binary patterns, we merge the two sets of patterns in dual phase-shifting method into a single

set of three-gray-level patterns. To preserve the speed advantage, we avoided introducing additional bits by binarizing the three-gray-level patterns with 2D modulation. Our simulation, quantitative experiment and qualitative experiment all demonstrate the performance enhancement of our proposed method especially when the projector is not sufficiently defocused.

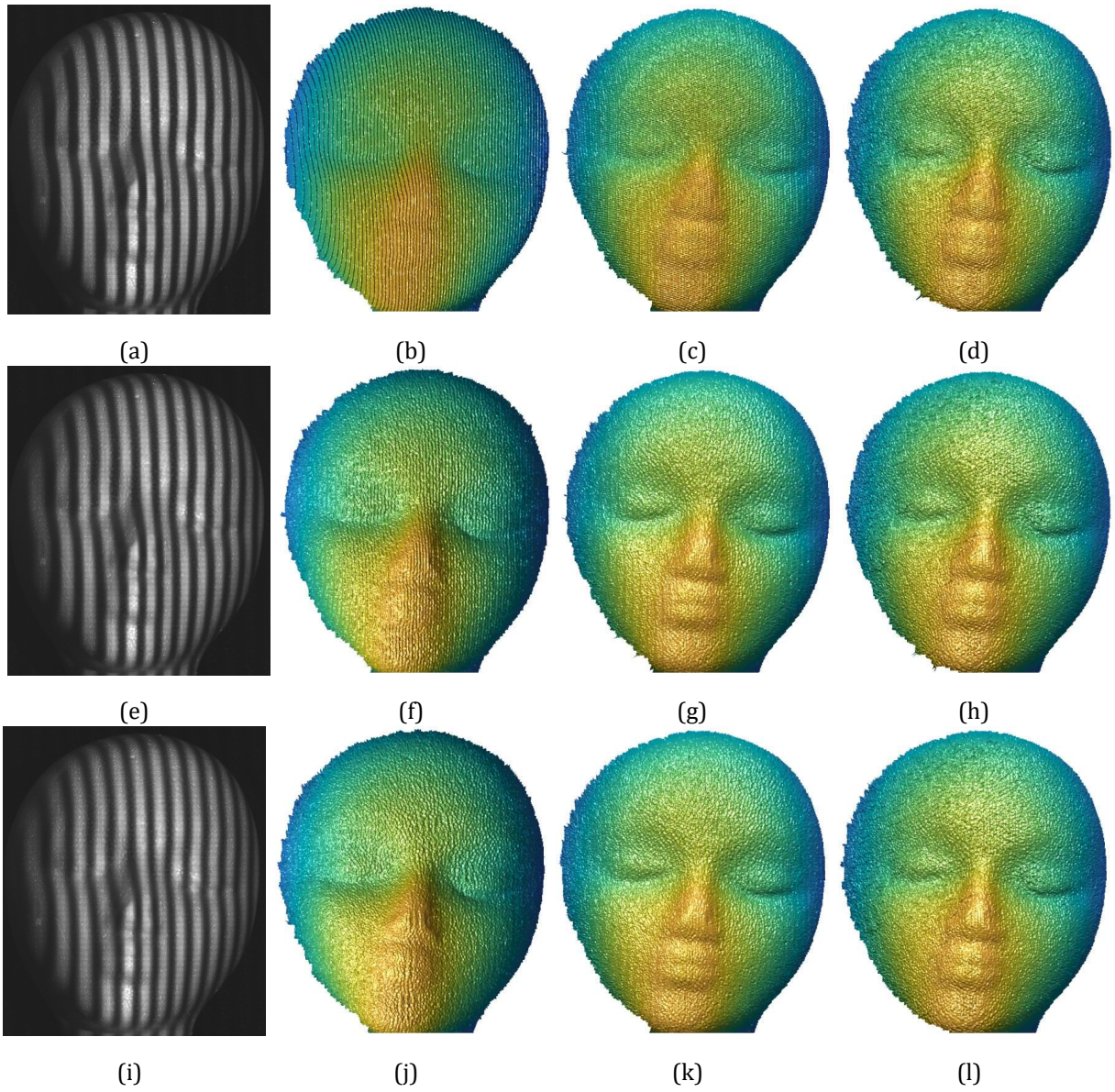

Figure 3.5 3D shape measurement of a sculpture head for visual comparison. (a) - (d) Figures showing the fringe image, the SPS result, the BDPS result and the HBDPS result when the projector is in-focus; (e) - (h) corresponding results when the projector is slightly defocused; (i) - (l) corresponding results when the projector is significantly defocused.

CHAPTER 4. SUMMARY AND FUTURE SCOPE OF WORK

In the previous chapter, we introduced our proposed binary dual phase shifting (BDPS) and Hilbert binary dual phase shifting (HBDPS) method for high-speed and high-quality 3-D shape measurements. This chapter summarizes the contribution of the research and provides discussions on some future scope of work.

4.1 Research Achievements

As both introduced in Chapter 1 and demonstrated in Chapter 3, we know that the level of defocus is a very important parameter for using binary patterns in 3-D measurement and reconstruction. It can be seen from the results demonstrated in Chapter 3 that when the projector is sufficiently defocused, the results are good even if we directly use the square binary patterns with the conventional single phase shifting method. However, if the projector is in-focus or slightly defocused, the phase error will be very high which leads to low quality measurement.

This thesis proposed BDPS and HBDPS methods the deal with such issue of using binary patterns with projector defocusing. In this research, simulations and experiments were conducted to compare the proposed methods to the more traditional techniques like single phase shifting method. Then, the experiments were conducted at three different levels of defocusing to determine the effectiveness the method proposed by us over the conventional single phase shifting method. Overall, the quality of the measurements for all aforementioned methods increase with the level of defocusing as expected, but the BDPS and HBDPS method are able to achieve higher quality than the conventional single phase shifting method even when the projector is not sufficiently defocused. Specifically, when the projector is in-focus,

the BDPS method reduces the harmonic errors by 47% and the HBDPS method reduces the harmonic errors by 74%.

Our proposed BDPS and HBDPS methods have several advantages compared to existing technologies. First of all, as aforementioned, it significantly enhanced the phase quality of the approach which directly uses square binary patterns with single phase shifting, especially when the projector is not sufficiently defocused. This leads to an increased effective range for projector defocusing when performing 3-D shape measurement with binary patterns. Moreover, our method still uses 1-bit binary structures in pattern design and did not increase the total number (i.e. 3) of patterns for phase retrieval. Therefore, the high-speed advantage of the binary technology is preserved. In a nutshell, our proposed BDPS and HBDPS methods have made contributions to promoting simultaneous high-speed and high-accuracy 3-D shape measurements.

4.2 Future scope of work

There are many areas where BDPS may be implemented. Here, we suggest a few per spective applications:

- *Face Recognition.* Face recognition and 3-D face reconstruction is common nowadays given that even phones and laptops having face recognition passwords. Researchers have tried using various techniques for high quality face recognition (Nagamine et al., 1992), (Lee and Yi, 2003),(Russ et al., 2004), etc. Although this a very popular topic for research, there are a few limitations (Bowyer et al., 2006) of the current technologies:

    1. Techniques are dependent upon ambient lighting.
    2. The person in question should be motionless and at a relative precise distance.

3. Limited ability to deliver good results for a variety of pose, expressions, even with minor changes like glasses, jewelries, etc.

We can try to overcome these limitations by using high-quality and high-speed 3D shape measurement and reconstruction. The requirement of the subject's to be motionless can solved by using a high-speed technique for real-time measurement and reconstruction. Since our technique does not require the projector to be sufficiently defocused, these techniques may be used to overcome the requirement of relatively precise distance of the subject. In the recent decade, there are research (Papatheodorou and Rueckert, 2004) going on to attempt to achieve 4-D face recognition. Our proposed method could be applicable to improving its efficiency and robustness by realizing simultaneous high-speed and high-quality 3D measurement.

- *Gaming and entertainment.* Gaming and entertainment industry is another field where 3-D imaging and reconstruction has potential applications. The technologies that are available nowadays like kinect and other real-time image acquisition and reconstruction techniques may lack enough accuracy which could lead to a non-veridical experience (Howarth, 2011). That is why games available nowadays usually uses a cartoon equivalent of the player. The next level of gaming could be actual real-life representation of the character in the virtual world. This requires a technique that are not only high speed, but also highly accurate as well. We can try to implement BDPS and HBDPS techniques to obtain data in the real world as they are able to achieve high-speed and high-quality 3-D shape measurements. Although for real life experience, more research is required, but utilization of these techniques for such applications could be a good stepping stone.

- *Optical Metrology for high speed in-line measurements.* Although the coordinate measuring machine (CMM) has been able to achieve very high accuracy in the order of μm level, but there are limitations of this method too. One of the major limitations is its slow processing speed. Hence this process is not applicable for making a quick decision. So, we need a technique which would be able to measure the parameters like surface roughness, dimensions of parts, etc., using non-contact techniques to make some quick decisions on the initial inspection. Although these measurements might not be able to reach an accuracy like CMM, but these techniques can be used to determine the disproportionate pieces for primary inspection. This will reduce the time of inspection greatly as in that case, only the parts that are meeting a minimum quality requirement need to be analyzed using CMM. The use of optical techniques here requires the technique to be able to achieve high accuracy; and for real time applications, it needs to be able to perform high-speed measurement along with high accuracy. Hence BDPS and HBDPS methods may have an opportunity for such applications. As can be seen in the previous chapter, phase error is very low in both proposed techniques even when the projector is in-focus. The fact that both techniques use 1-bit patterns will make these techniques suitable for a quick inspection.

BIBLIOGRAPHY

Albarelli, A., Rodola`, E., and Torsello, A. (2009). Robust camera calibration using inaccurate targets. *IEEE Trans. Pattern Anal. Mach. Intell.*, 31:376–383.

Armbruster, K. and Scheffler, M. (1998). Messendes 3d-endoskop.

Ayubi, G. A., Ayubi, J. A., Di Martino, J. M., and Ferrari, J. A. (2010). Pulse-width modulation in defocused three-dimensional fringe projection. *Optics letters*, 35(21):3682– 3684.

Bell, T., Li, B., and Zhang, S. (2016). Structured light techniques and applications. *Wiley Encyclopedia of Electrical and Electronics Engineering*.

Bhatia, G., Vannier, M. W., Smith, K. E., Commean, P. K., Riolo, J., and Young, V. L. (1994). Quantification of facial surface change using a structured light scanner. *Plastic and reconstructive surgery*, 94(6):768–774.

Bitte, F., Dussler, G., and Pfeifer, T. (2001). 3d micro-inspection goes dmd. *Optics and lasers in engineering*, 36(2):155–167.

Bowyer, K. W., Chang, K., and Flynn, P. (2006). A survey of approaches and challenges in 3d and multi-modal 3d+ 2d face recognition. *Computer vision and image understanding*, 101(1):1–15.

Bush, K. and Antonyshyn, O. (1996). Three-dimensional facial anthropometry using a laser surface scanner: validation of the technique. *Plastic and reconstructive surgery*, 98(2):226–235.

Cai, Z., Liu, X., Jiang, H., He, D., Peng, X., Huang, S., and Zhang, Z. (2015). Flexible phase error compensation based on hilbert transform in phase shifting profilometry. *Optics express*, 23(19):25171–25181.

Chazan, G. and Kiryati, N. (1995). *Pyramidal intensity-ratio depth sensor*. Technion-IIT, Department of Electrical Engineering.

Chen, C.-W. and Chen, Y.-Y. (2011). Recovering depth from a single image using spectral energy of the defocused step edge gradient. In *Image Processing (ICIP), 2011 18th IEEE International Conference on*, pages 1981–1984. IEEE.

Costantini, M. (1998). A novel phase unwrapping method based on network programming. *IEEE Transactions on geoscience and remote sensing*, 36(3):813–821.

Dai, J., Li, B., and Zhang, S. (2014). High-quality fringe pattern generation using binary pattern optimization through symmetry and periodicity. *Optics and Lasers in Engineering*, 52:195–200.

Dai, J. and Zhang, S. (2013). Phase-optimized dithering technique for high-quality 3d shape measurement. *Optics and Lasers in Engineering*, 51(6):790–795.

Dhond, U. R. and Aggarwal, J. K. (1989). Structure from stereo-a review. *IEEE transactions on systems, man, and cybernetics*, 19(6):1489–1510.

Ding, Y., Xi, J., Yu, Y., and Chicharo, J. (2011). Recovering the absolute phase maps of two fringe patterns with selected frequencies. *Optics letters*, 36(13):2518–2520.

Ding, Y., Xi, J., Yu, Y., and Deng, F. (2015). Absolute phase recovery of three fringe patterns with selected spatial frequencies. *Optics and Lasers in Engineering*, 70:18–25.

Duane, C. B. (1971). Close-range camera calibration. *Photogramm. Eng*, 37(8):855–866.

Farkas, L. G., Hajniˇs, K., and Posnick, J. C. (1993). Anthropometric and anthroposcopic findings of the nasal and facial region in cleft patients before and after primary lip and palate repair. *The Cleft palate-craniofacial journal*, 30(1):1–12.

Favaro, P. and Soatto, S. (2005). A geometric approach to shape from defocus. *IEEE Transactions on Pattern Analysis and Machine Intelligence*, 27(3):406–417.

Favaro, P., Soatto, S., Burger, M., and Osher, S. J. (2008). Shape from defocus via diffusion. *IEEE transactions on pattern analysis and machine intelligence*, 30(3):518–531.

Ferrario, V. F., Sforza, C., Poggio, C. E., Cova, M., and Tartaglia, G. (1998). Preliminary evaluation of an electromagnetic three-dimensional digitizer in facial anthropometry. *The Cleft palate-craniofacial journal*, 35(1):9–15.

Geng, J. (2011). Structured-light 3d surface imaging: a tutorial. *Advances in Optics and Photonics*, 3(2):128–160.

Ghiglia, D. C. and Pritt, M. D. (1998). *Two-dimensional phase unwrapping: theory, algorithms, and software*, volume 4. Wiley New York.

Gonzalez-Jorge, H., Riveiro, B., Vazquez-Fernandez, E., Mart´ınez-Sa´nchez, J., and Arias, P. (2013). Metrological evaluation of microsoft kinect and asus xtion sensors. *Measurement*, 46(6):1800–1806.

Gonzalez-Jorge, H., Rodr´ıguez-Gonz´alvez, P., Mart´ınez-S´anchez, J., Gonza´lez-Aguilera, D., Arias, P., Gesto, M., and D´ıaz-Vilarin˜o, L. (2015). Metrological comparison between kinect i and kinect ii sensors. *Measurement*, 70:21–26.

Gorthi, S. S. and Rastogi, P. (2010). Fringe projection techniques: whither we are? *Optics and lasers in engineering*, 48(IMAC-REVIEW-2009-001):133–140.

Guo, H., Chen, M., and Zheng, P. (2006). Least-squares fitting of carrier phase distribution by using a rational function in fringe projection profilometry. *Optics letters*, 31(24):3588–3590.

Hornbeck, L. J. (1997). Digital light processing for high-brightness high-resolution applications. In *Projection Displays III*, volume 3013, pages 27–41. International Society for Optics and Photonics.

Hornbeck, L. J. (1999). Digital light processing update: status and future applications. In *Projection Displays V*, volume 3634, pages 158–171. International Society for Optics and Photonics.

Howarth, P. A. (2011). Potential hazards of viewing 3-d stereoscopic television, cinema and computer games: a review. *Ophthalmic and Physiological Optics*, 31(2):111–122.

Hu, Q., Huang, P. S., Fu, Q., and Chiang, F.-P. (2003). Calibration of a three-dimensional shape measurement system. *Optical Engineering*, 42(2):487–494.

Huang, L., Zhang, Q., and Asundi, A. (2013). Flexible camera calibration using not-measured imperfect target. *Applied optics*, 52(25):6278–6286.

Huang, P. S. and Zhang, S. (2006). Fast three-step phase-shifting algorithm. *Applied optics*, 45(21):5086–5091.

Hyun, J.-S. and Zhang, S. (2016). Enhanced two-frequency phase-shifting method. *Applied optics*, 55(16):4395–4401.

Judge, T. R. and Bryanston-Cross, P. (1994). A review of phase unwrapping techniques in fringe analysis. *Optics and Lasers in Engineering*, 21(4):199–239.

Lavest, J.-M., Viala, M., and Dhome, M. (1998). Do we really need an accurate calibration pattern to achieve a reliable camera calibration? In *European Conference on Computer Vision*, pages 158–174. Springer.

Lee, Y. and Yi, T. (2003). 3d face recognition using multiple features for local depth information. In *Video/Image Processing and Multimedia Communications, 2003. 4th EURASIP Conference focused on*, volume 1, pages 429–434. IEEE.

Legarda-Sa´enz, R., Bothe, T., and Ju¨ptner, W. P. (2004). Accurate procedure for the calibration of a structured light system. *Optical Engineering*, 43(2):464–472.

Lei, S. and Zhang, S. (2009). Flexible 3-d shape measurement using projector defocusing. *Optics letters*, 34(20):3080–3082.

Levin, A., Fergus, R., Durand, F., and Freeman, W. T. (2007). Image and depth from a conventional camera with a coded aperture. *ACM transactions on graphics (TOG)*,

26(3):70.

Li, B. (2014). High quality three-dimensional (3d) shape measurement using intensityoptimized dithering technique.

Li, B. and Zhang, S. (2014). Structured light system calibration method with optimal fringe angle. *Applied optics*, 53(33):7942–7950.

Li, Z., Shi, Y., Wang, C., and Wang, Y. (2008). Accurate calibration method for a structured light system. *Optical Engineering*, 47(5):053604.

Lin, J., Ji, X., Xu, W., and Dai, Q. (2013). Absolute depth estimation from a single defocused image. *IEEE Transactions on Image Processing*, 22(11):4545–4550.

Lohry, W. and Zhang, S. (2012). 3d shape measurement with 2d area modulated binary patterns. *Optics and Lasers in Engineering*, 50(7):917–921.

Malacara, D. (2007). *Optical shop testing*, volume 59. John Wiley & Sons.

Mao, X., Chen, W., and Su, X. (2007). Improved fourier-transform profilometry. *Applied optics*, 46(5):664–668.

McGovern, A. C., Broadhurst, D., Taylor, J., Kaderbhai, N., Winson, M. K., Small, D. A., Rowland, J. J., Kell, D. B., and Goodacre, R. (2002). Monitoring of complex industrial bioprocesses for metabolite concentrations using modern spectroscopies and machine learning: application to gibberellic acid production. *Biotechnology and Bioengineering*, 78(5):527–538.

McMurtry, D. R. (1982). Coordinate measuring machine. US Patent 4,333,238.

Mehta, R. P., Zhang, S., and Hadlock, T. A. (2008). Novel 3-d video for quantification of facial movement. *OtolaryngologyHead and Neck Surgery*, 138(4):468–472.

Menna, F., Remondino, F., Battisti, R., and Nocerino, E. (2011). Geometric investigation of a gaming active device. In *Videometrics, Range Imaging, and Applications XI*, volume 8085, page 80850G. International Society for Optics and Photonics.

Nagamine, T., Uemura, T., and Masuda, I. (1992). 3d facial image analysis for human identification. In *Pattern Recognition, 1992. Vol. I. Conference A: Computer Vision and Applications, Proceedings., 11th IAPR International Conference on*, pages 324–327. IEEE.

Namboodiri, V. P. and Chaudhuri, S. (2008). Recovery of relative depth from a single observation using an uncalibrated (real-aperture) camera. In *Computer Vision and Pattern Recognition, 2008. CVPR 2008. IEEE Conference on*, pages 1–6. IEEE.

Olesen, O. V., Paulsen, R. R., Hojgaard, L., Roed, B., and Larsen, R. (2012). Motion tracking for medical imaging: a nonvisible structured light tracking approach. *IEEE transactions on medical imaging*, 31(1):79–87.

Pages, J., Salvi, J., Collewet, C., and Forest, J. (2005). Optimised de bruijn patterns for one-shot shape acquisition. *Image and Vision Computing*, 23(8):707–720.

Pages, J., Salvi, J., and Forest, J. (2004). A new optimised de bruijn coding strategy for structured light patterns. In *Pattern Recognition, 2004. ICPR 2004. Proceedings of the 17th International Conference on*, volume 4, pages 284–287. IEEE.

Pagliari, D., Menna, F., Roncella, R., Remondino, F., and Pinto, L. (2014). Kinect fusion improvement using depth camera calibration. *The International Archives of Photogrammetry, Remote Sensing and Spatial Information Sciences*, 40(5):479.

Papatheodorou, T. and Rueckert, D. (2004). Evaluation of automatic 4d face recognition using surface and texture registration. In *Automatic Face and Gesture Recognition, 2004. Proceedings. Sixth IEEE International Conference on*, pages 321–326. IEEE.

Payeur, P. and Desjardins, D. (2009). Structured light stereoscopic imaging with dynamic pseudo-random patterns. In *International Conference Image Analysis and Recognition*, pages 687–696. Springer.

Pettersson, B. (2009). Coordinate measuring machine. US Patent 7,591,077.

Pettigrew, R. M. (1988). Displacement measuring apparatus and method.

Pfeifer, T. and Effenkammer, D. (2000). Demands on manufacturing metrology and solutions. In *Proceedings of the XVI IMEKO World Congress, Vienna, Austria*, volume 8, pages 231– 236.

Rajagopalan, A. N. and Chaudhuri, S. (1999). An mrf model-based approach to simultaneous recovery of depth and restoration from defocused images. *IEEE transactions on pattern analysis and machine intelligence*, 21(7):577–589.

Rajan, D. and Chaudhuri, S. (2003). Simultaneous estimation of super-resolved scene and depth map from low resolution defocused observations. *IEEE Transactions on Pattern Analysis and Machine Intelligence*, 25(9):1102–1117.

Russ, T. D., Koch, M. W., and Little, C. Q. (2004). 3d facial recognition: a quantitative analysis. In *Security Technology, 2004. 38th Annual 2004 International Carnahan Conference on*, pages 338–344. IEEE.

Salvi, J., Pages, J., and Batlle, J. (2004). Pattern codification strategies in structured light systems. *Pattern recognition*, 37(4):827–849.

Sansoni, G., Trebeschi, M., and Docchio, F. (2009). State-of-the-art and applications of 3d imaging sensors in industry, cultural heritage, medicine, and criminal investigation. *Sensors*, 9(1):568–601.

Scharstein, D. and Szeliski, R. (2002). A taxonomy and evaluation of dense two-frame stereo correspondence algorithms. *International journal of computer vision*, 47(1-3):7–42.

Schechner, Y. Y. and Kiryati, N. (2000). Depth from defocus vs. stereo: How different really are they? *International Journal of Computer Vision*, 39(2):141–162.

Sobel, I. (1974). On calibrating computer controlled cameras for perceiving 3-d scenes. *Artificial Intelligence*, 5(2):185–198.

Song, Z. and Chung, R. (2008). Grid point extraction exploiting point symmetry in a pseudorandom color pattern. In *Image Processing, 2008. ICIP 2008. 15th IEEE International Conference on*, pages 1956–1959. IEEE.

Srinivasan, V., Liu, H.-C., and Halioua, M. (1984). Automated phase-measuring profilometry of 3-d diffuse objects. *Applied optics*, 23(18):3105–3108.

Strobl, K. H. and Hirzinger, G. (2011). More accurate pinhole camera calibration with imperfect planar target. In *Computer Vision Workshops (ICCV Workshops), 2011 IEEE International Conference on*, pages 1068–1075. IEEE.

Subbarao, Mura**li** and Surya, G. (1994). Depth from defocus: a spatial domain approach. *International Journal of Computer Vision*, 13(3):271–294.

Takeda, M. and Mutoh, K. (1983). Fourier transform profilometry for the automatic measurement of 3-d object shapes. *Applied optics*, 22(24):3977–3982.

Trouve, E., Nicolas, J.-M., and Maitre, H. (1998). Improving phase unwrapping techniques by the use of local frequency estimates. *IEEE Transactions on geoscience and remote sensing*, 36(6):1963–1972.

Tsai, R. (1987). A versatile camera calibration technique for high-accuracy 3d machine vision metrology using off-the-shelf tv cameras and lenses. *IEEE Journal on Robotics and Automation*, 3(4):323–344.

Vermeulen, M., Rosielle, P., and Schellekens, P. (1998). Design of a high-precision 3dcoordinate measuring machine. *CIRP Annals-Manufacturing Technology*, 47(1):447–450.

Vo, M., Wang, Z., Pan, B., and Pan, T. (2012). Hyper-accurate flexible calibration technique for fringe-projection-based three-dimensional imaging. *Optics Express*, 20(15):16926– 16941.

Wang, Y. and Zhang, S. (2010). Optimal pulse width modulation for sinusoidal fringe generation with projector defocusing. *Optics letters*, 35(24):4121–4123.

Wang, Y. and Zhang, S. (2012a). Novel phase-coding method for absolute phase retrieval. *Optics letters*, 37(11):2067–2069.

Wang, Y. and Zhang, S. (2012b).Three-dimensional shape measurement with binary dithered patterns. *Applied optics*, 51(27):6631–6636.

Watanabe, M. and Nayar, S. K. (1998). Rational filters for passive depth from defocus. *International Journal of Computer Vision*, 27(3):203–225.

Xu, Y., Ekstrand, L., Dai, J., and Zhang, S. (2011). Phase error compensation for threedimensional shape measurement with projector defocusing. *Applied Optics*, 50(17):2572– 2581.

Yin, Y., Peng, X., Li, A., Liu, X., and Gao, B. Z. (2012). Calibration of fringe projection profilometry with bundle adjustment strategy. *Optics letters*, 37(4):542–544.

Zhang, S. (2011). High-resolution 3d profilometry with binary phase-shifting methods. *Applied optics*, 50(12):1753–1757.

Zhang, S. (2012). Composite phase-shifting algorithm for absolute phase measurement.

Optics and Lasers in Engineering, 50(11):1538–1541.

Zhang, S. and Huang, P. S. (2006). Novel method for structured light system calibration. *Optical Engineering*, 45(8):083601.

Zhang, S., Van Der Weide, D., and Oliver, J. (2010). Superfast phase-shifting method for 3-d shape measurement. *Optics express*, 18(9):9684–9689.

Zhang, Z. (2000). A flexible new technique for camera calibration. *IEEE Transactions on pattern analysis and machine intelligence*, 22(11):1330–1334.

Zuo, C., Chen, Q., Feng, S., Feng, F., Gu, G., and Sui, X. (2012). Optimized pulse width modulation pattern strategy for three-dimensional profilometry with projector defocusing.*Applied optics*, 51(19):4477–4490.